PHYSICAL REVIEW C VOLUME 9, NUMBER 3 MARCH 1974

Lifetime measurements and $E2$ effective charges for nuclei in the $1f_{7/2}$ shell*

B. A. Brown, D. B. Fossan, J. M. McDonald,† and K. A. Snover‡
Department of Physics, State University of New York, Stony Brook, New York 11790
(Received 5 October 1973)

Lifetimes for a number of levels in nuclei with $40 < A < 56$ have been measured using the recoil-distance technique. The experimental results for the mean lifetimes are 45^{+10}_{-7} psec for the 1491-keV 3^+ and 57 ± 10 psec for the 1511-keV 5^+ levels in ^{42}Sc; 8.1 ± 1.1 psec for the 2987-keV $\frac{15}{2}^-$ level in ^{43}Sc; 19.6 ± 1.7 psec for the 3285-keV 6^+ level in ^{44}Ca; 12.8 ± 1.2 psec for the 3334-keV 6^+ level in ^{48}Ti; 5.1 ± 1.0 psec for the 1021-keV $\frac{11}{2}^-$ level in ^{49}V; 12.6 ± 2.1 psec for the 783-keV 2^+ level in ^{50}Cr; 20.4 ± 3.3 psec for the 238-keV $\frac{7}{2}^-$ level in ^{51}Mn; $13.7^{+3.6}_{-2.3}$ psec for the 2369-keV 4^+_1, 59.5 ± 3.3 psec for the 3114-keV 6^+, and 10.4 ± 1.2 psec for the 3469-keV $(3^\pm, 5^-)$ levels in ^{52}Cr; 15.5 ± 1.8 psec for the 2563-keV $\frac{13}{2}^-$ and 3.9 ± 0.6 psec for the 2693-keV $\frac{15}{2}^-$ levels in ^{53}Mn; and 5.7 ± 1.2 psec for the 2538-keV 4^+ level in ^{54}Fe. Lifetime limits were found for eight additional levels in these nuclei. In addition, an improved value $\tau = 68.3\pm3.1$ psec was obtained for 937-keV 3^+ level in ^{18}F. The $B(E2)$ strengths for transitions in nuclei with $42 \le A \le 44$ are collected and interpreted in terms of isospin-dependent effective charges using wave functions for the $(1f_{7/2})^n$, and $(fp)^n$, and $(fp)^{n+m}(sd)^{-m}$ model spaces. The core-polarization charges obtained from an analysis using $(fp)^2 + (fp)^4(sd)^{-2}$ wave functions are $e_p = 1.16\pm0.16$ and $e_n = 0.45\pm0.03$. Core-deformation effects are found to enhance the isoscalar but not the isovector effective charges for states with low spin. The $B(E2)$ strengths for transitions in the isotones with 28 neutrons are also collected and interpreted using $(1f_{7/2})^n$ wave functions. The effective proton charge is found to be approximately constant for all transitions with $e_p = 1.8 - 2.0$. Estimates of effective proton charges for these nuclei resulting from the use of larger model spaces are discussed allowing an approximate comparison for the whole $40 < A < 56$ region.

[NUCLEAR REACTIONS ^{39}K(α,n) E=10.4 MeV, ^{40}Ca$(^3$He$,p)$ E=10.5 MeV, ^{16}O$(^3$He$,p)$ E=10.5 MeV, ^{40}Ca(α,p) E=14.0 MeV, ^{41}K(α,p) E=14.0 MeV, ^{45}Sc(α,p) E=10.0 MeV, ^{46}Ti(α,p) E=11.0 MeV, ^{40}Ca$(^{16}$O$,\alpha 2p)$ E=47 MeV, ^{49}Ti(α,n) E=14.5 MeV, ^{40}Ca$(^{16}$O$,3p)$ E=47 MeV, ^{40}Ca$(^{16}$O$,2p)$ E=47 MeV; measured recoil distance. Deduced $T_{1/2}$, $B(E2)$. Deduced $40 < A < 56$ effective charges. Natural and enriched targets, Ge(Li) detector.]

I. INTRODUCTION

Effective multipole operators have been successfully used to account for core-polarization contributions to $E2$ γ-ray transitions in nuclei.[1] The polarization of the charged core, which results from particles outside the closed shells (valence particles), involves virtual excitations of core particles into orbitals at energies $2\hbar\omega$ higher. The core-polarization contributions are incorporated into the effective operators by changing the charge of the valence particles into effective charges.

The $E2$ effective charges are expected to be independent of the number of similar valence particles, namely additive, since the admixture of core excitations due to one valence particle is small. Any state dependence of the effective charges resulting from different valence orbitals, although not large, must be considered. In addition, because of the isovector interaction between the charged core and a valence nucleon, the effective charges can be different for neutrons and protons, that is, isospin dependent. This isospin dependence is particularly interesting because of its relation to the isospin structure of the giant resonances. The properties of effective charges have been carefully studied in the region around ^{208}Pb by Astner *et al.*[2]; this region is particularly suitable because of the purity of the wave functions.

The purpose of the present experiment is to explore the $E2$ effective charges in the region of $40 < A < 56$ where the $1f_{7/2}$ shell is of dominant importance. Since the wave functions in this region contain certain admixtures from the upper part of the $1f$-$2p$ shell and the closed $1s$-$2d$ shell, special consideration must be given in the effective charge analysis for different shell-model truncations and effective interactions. This can be circumvented partially by studying transitions between high-spin states where the admixtures into the $(1f_{7/2})^n$ configurations are small. Recent microscopic calculations of the $E2$ effective charges near ^{40}Ca by Kuo and Osnes[3] adds special interest to this experimental investigation.

In the present experiment, lifetimes of high-spin states in the $40 < A < 56$ region are measured from which $E2$ transition strengths are extracted. The recoil-distance technique has been used to measure a number of transitions of interest which fall into the mean-life range of a few psec to 100 psec. These new lifetime results together with previous Doppler-shift attenuation method (DSAM) measurements for τ less than a few psec and electronic measurements for $\tau \gtrsim 100$ psec form a fairly complete set of $B(E2)$ values for high-spin states from which the evaluation of $E2$ effective charges are made. These effective charge results are then compared with several theoretical predictions. The details of the present experiment are discussed in Sec. II and the lifetime results are presented in Sec. III. Sec. IV contains a description of the various approaches used in the extraction of the effective charges and a presentation of the effective-charge systematics. Conclusions regarding the effective charges including comparisons between the observed effective charges and the theoretical predictions are given in Sec. V.

II. EXPERIMENTAL TECHNIQUE

The recoil-distance (plunger) technique[4-6] has been used to measure lifetimes of various levels of interest in $1f_{7/2}$-shell nuclei. The plunger apparatus used for these measurements was described previously.[5] These levels were populated via nuclear reactions induced by α-, ^{3}He-, and ^{16}O-particle beams from the Stony Brook tandem Van de Graaff accelerator. The targets from 20 to 260 μg/cm^2 thickness were evaporated onto 3-mg/cm^2 Au backing foils. They were oriented with the Au foil facing the beam and positioned in the plunger apparatus by means of a V-groove, O-ring arrangement designed to hold the target flat. The recoiling excited nuclei from, for example, the (α,n) and (α,p) reactions which were used for the majority of the present measurements, were kinematically confined to a forward cone with half angles ranging from 17 to 28°. In most cases, the targets were made about a factor of 2 thinner than the approximate target range for the minimum recoil energy, so that all the recoiling ions leave the target with a significant velocity.

The excited nuclei, which recoil with a velocity component v in the direction of the beam and decay of flight, will emit γ rays at 0° to the beam with a shifted energy $E_s = E_0(1+v/c)$. A flat Au plunger positioned at a distance $D-D_0$ from the target stops the recoiling nuclei so that those which decay at a time greater than the flight time $t=(D-D_0)/v$ will emit γ rays with an unshifted energy E_0. The γ-ray energy spectra were measured for various plunger distances with a 45-cm^3 Ge(Li) detector at 0°. The detector energy resolution was about 2.5 keV at 1332 keV, which was generally sufficient to resolve the γ-ray peaks at energies E_0 and E_s (typically $E_s - E_0 \sim 6$ keV for $E_0 = 1$ MeV). The corresponding peak areas I_0 and I_s were determined for the appropriate decay γ rays by a simultaneous least-squares fit to Gaussian and skew-Gaussian shapes respectively, along with a polynomial fitted to the background. The experimental ratios R of the unshifted peak area to the total area, $I_0/(I_0+I_s)$, were then formed from measurements at each distance.

To illustrate this analysis for a typical case, the γ-ray data for the $\frac{15}{2}^-$ level ($\frac{15}{2}^- \to \frac{11}{2}^-$, 1157-keV transition) in ^{43}Sc obtained via the ^{40}Ca$(\alpha,p)^{43}$Sc reaction ($E_\alpha = 14.0$ MeV, 48-μg/cm^2 natural Ca metal target on Au backing) are shown in the left half of Fig. 1 for three plunger distances $D-D_0$. The maximum recoil half angle is 20° and the resulting mean recoil velocity which was obtained from the difference in centroid energies of I_0 and I_s at 0° is $\bar{v}/c = 0.65\%$ ($\bar{v} = 1.9$ μm/psec). The solid curve through the γ-ray spectra represents the computer fits for $I_0 + I_s$ and the background; the fitted background is also shown under the peak areas. The dashed lines give the individual contributions for I_0 and I_s. The ratios $R - R_\infty$ obtained at the different plunger distances are plotted with error bars as a function of distance in the right half of Fig. 1. A small background ratio R_∞ which can be due, for instance, to nuclear stopping in the target material is usually observed at large distances. In this ^{43}Sc illustration, there is a significant R_∞ due to cascade feeding from the long-lived $\frac{19}{2}^-$ level ($\tau = 650$ nsec).

In order to express the ratio R in terms of the nuclear lifetime, a knowledge of the recoil velocities is required. If all of the nuclei recoil with the same velocity v, then $I_0 = Ne^{-(D-D_0)/v\tau}$, where τ is the mean lifetime, and the ratio R is given by $R = e^{-(D-D_0)/v\tau}$ since $I_0 + I_s = N$. In practice there is a spread in the recoil velocities resulting from the kinematics and target thickness. Thus the experimental ratios obtained as a function of D were fitted with the following formula[5]:

$$R(D-D_0) = A \sum_i a_i e^{-(D-D_0)v_i \tau} + R_\infty , \qquad (1)$$

where $A + R_\infty = 1$ so that $R(0) = 1$. The background ratio R_∞ is measured with good statistical accuracy at a distance $D \gg v\tau$. The a_i represents the fraction of nuclei recoiling with velocity v_i (normalized such that $\sum_i a_i = 1$) and are determined from the experimental shape of the shifted peak after unfolding the detector resolution taken to have a Gaussian shape. The shape of the shifted peak, due to the presence of a spread in recoil velocities, was found from spectra taken at large plunger distances. The parameters τ, D_0, and R_∞ were allowed to vary in fitting each ratio curve. The solid curve in the right half of Fig. 1 corresponding to $\tau = 8.1 \pm 1.1$ psec represents this best fit for the $\frac{15}{2}^-$ level in ^{43}Sc. The lifetime values obtained using Eq. (1) usually differed only a few percent from the lifetimes determined from the first-order equation

$$R = Ae^{-(D-D_0)/\bar{v}\tau} + R_\infty , \tag{2}$$

where $\bar{v}$ is the mean recoil velocity. This close agreement is due to the fact that the spread in recoil velocities was generally small for these measurements. The first-order fit with Eq. (2) for the ^{43}Sc example yielded $\tau = 8.4 \pm 1.1$ psec, which is only a 3% difference from the fit with Eq. (1). In the event that either I_0 or I_s are obscured by contaminants in the γ-ray spectra, a decay curve can usually be obtained by normalizing either I_0 or I_s to another transition in the spectra which has an intensity proportional to that of the transition of interest.

Several small corrections[5,6] must be applied to lifetime values extracted in the manner described above. The corrections for the finite solid angle of the detector and the efficiency variation for the I_0 and I_s peaks are generally small (<1% for the present measurements) and are applied to the value of the lifetime since they are accurately known. For the ^{43}Sc $\frac{15}{2}^-$ level, the sum of these two corrections to the lifetime was only 0.1%. The effect of a possible distribution of distances $(D - D_0)$ in the plunger apparatus (due, for example, to a nonparallel plunger and target) was only a few percent in the worst cases and was folded into the lifetime uncertainty. It has been shown[5] that the presence of a distance distribution in the absence of a velocity distribution does not effect the extracted lifetime.

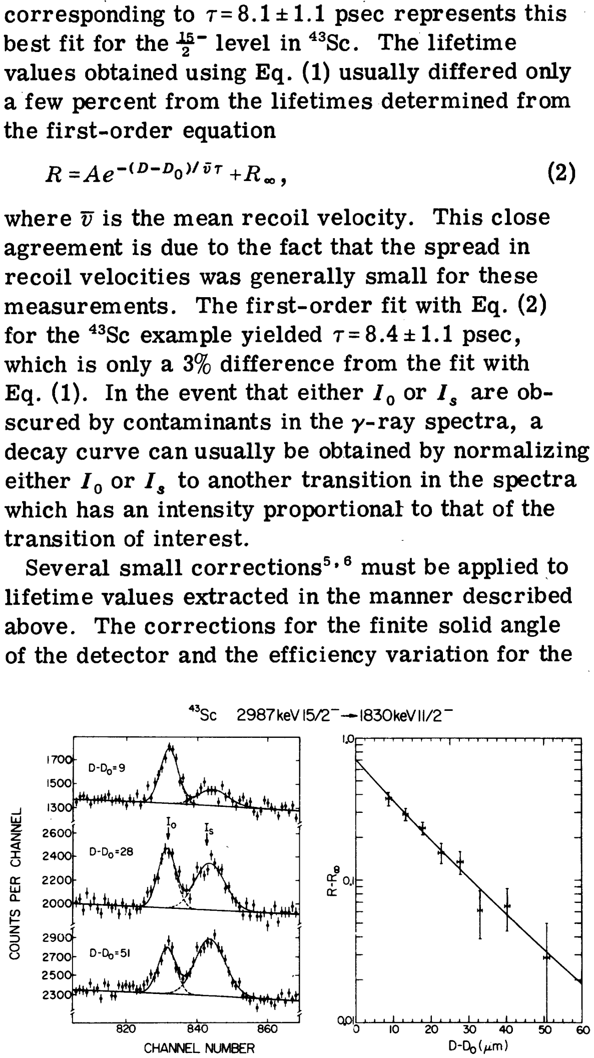

FIG. 1. Recoil-distance γ-ray spectra and lifetime decay curve for the ^{43}Sc 2987-keV $\frac{15}{2}^- \rightarrow$ 1830-keV $\frac{11}{2}^-$ transition. The left portion of the figure displays the γ-ray spectra in the region of the 1157-keV transition measured at three different plunger distances, $D - D_0$ in μm, with I_0 and I_S indicating the stopped and shifted peaks, respectively. The methods of extracting the I_0 and I_S areas are discussed in the text. The right portion of the figure is a semilogarithmic plot of $R - R_\infty$ vs $D - D_0$ where $R = I_0/(I_0 + I_S)$. The curve through the ratio data represents a least-squares fit of Eq. (1) to the data as described in the text.

Corrections to the measured lifetimes for the deorientation effect must also be considered.[5-7] It is well known that the angular distributions of γ rays from the decay of excited nuclei which recoil into vacuum can be attenuated as a result of the interaction between the nucleus and the atomic hyperfine fields. That is, the angular distribution parameters A_k are reduced in time by the multiplicative factors $G_k(t)$. Assuming that $G_k(t) = e^{-\lambda_k t}$ for $t < (D - D_0)/\bar{v}$ and $G_k(t = (D - D_0)/\bar{v})$ for $t \geq (D - D_0)/\bar{v}$ where $(D - D_0)/\bar{v}$ is the flight time of the nucleus, the ratio R for detection of γ rays at 0° is given by

$$R = \frac{e^{-\lambda(D-D_0)/\bar{v}} + \sum_k A_k e^{-\lambda_k (D-D_0)/\bar{v}}}{1 + \sum_k A_k [\lambda/\lambda_k' + (1 - \lambda/\lambda_k') e^{-\lambda'(D-D_0)/\bar{v}}]} , \tag{3}$$

where $\lambda = 1/\tau$ and $\lambda_k' = \lambda + \lambda_k$.

By the theory of Abragam and Pound,[8] $\lambda_k = k(k+1)\omega^2\tau_c/3$ where τ_c is the mean fluctuation time of the hyperfine interaction and $\omega = \mu_N gH/\hbar$ assuming a magnetic dipole interaction. The quantity $\omega^2\tau_c$ has been measured by Häusser *et al.*[9] to be 4×10^{10} sec^{-1} for Ti isotopes with a recoil velocity of $v/c = 0.046$. Assuming that the magnetic hyperfine field H is proportional to $Z(v/c)^x$ and using similar values of τ_c and g, the parameters λ_k can be extracted for the present measurements using the exponent measured by Häusser *et al.* ($x = 0.95 \pm 0.30$). This estimation of the λ_k is approximate; however, the deorientation lifetimes $\tau_2 = 1/\lambda_2$ determined in the above manner are at least a factor of 2 larger than the present lifetime values. For this reason the deorientation effect has been taken as an additional uncertainty with the parameters A_k and λ_k determined in a "worst" case, namely for A_k values corresponding to maximum alignment and for λ_k values determined with $x = 0.6$. The additional error was typically on the order of 1% while in a few cases for the longer lifetimes it was about 5%. In the case of the ^{43}Sc example, the deorientation lifetimes τ_k are 139 and 41 psec, respectively, for $k = 2$ and 4 which are considerably larger than the lifetime and thus yield a negligible correction.

The measurements described herein were singles measurements in which only the γ ray has been detected. In order to obtain a sufficient counting rate, it was necessary, in most cases, to make these measurements at bombarding energies appreciably higher than the kinematic threshold for production of the level of interest. Hence, the question of feeding from higher levels must be considered. The first-order equation that describes the ratio R for a level that is fed both directly from a reaction and indirectly from a second level at higher energy is

$$R = A\{fe^{-(D-D_0)/\bar{v}\tau} + [f'/(\tau' - \tau)] \times [\tau' e^{-(D-D_0)/\bar{v}'\tau'} - \tau e^{-(D-D_0)/\bar{v}'\tau}]\} + R_\infty . \tag{4}$$

The f and f' are, respectively, the direct and cascade population fractions ($f + f' = 1$), and $\bar{v}$ and $\bar{v}'$ are the mean recoil velocities corresponding to the population of each level. Cascades from highly excited levels are generally associated with short lifetimes $\tau' \ll \tau$, in which case, Eq. (4) reduces, for times $(D - D_0)/\bar{v}$ of the order of τ and with $\bar{v} \approx \bar{v}'$, to the equation for direct population, Eq. (2). If the feeding level has a lifetime longer than τ, namely $\tau' \gg \tau$, then Eq. (4) reduces to $R = A[fe^{-(D-D_0)/\bar{v}\tau} + f'] + R_\infty$. This result is also represented by Eq. (2) provided the term Af' is absorbed into R_∞ and D_0 includes an apparent shift $\Delta D_0 = \bar{v}\tau \ln f$. Thus for partial feeding from levels with lifetimes τ' that are either much greater or less than τ, the correct lifetime τ is obtained by fitting the decay curve with Eq. (2).

In a cascade feeding situation where τ' is of the same order as τ, the decay curve contains the influence of both lifetimes. To fit such data, the complete Eq. (4) is required; an erroneous lifetime would be obtained in this case with a fit to Eq. (2). To insure that any feeding levels did not influence the measured decay curves, the lifetimes associated with all cascade γ rays that feed the levels of interest were examined in the plunger data, in addition to checking for near linearity in the logarithmic decay curve. In some cases lifetimes of certain levels could not be extracted because of the possibility of unidentified cascade transitions of appreciable intensity. In the case of ^{42}Sc, where the transitions of interest were very weak and it was difficult to apply such tests, several measurements including threshold studies were made under a variety of conditions to help ensure the reliability of these results. For one level in ^{52}Cr, Eq. (4) was required to extract the appropriate lifetime τ after measuring the lifetime τ' of a feeding level.

III. EXPERIMENTAL RESULTS

The experimental results for the current recoil-distance measurements in $1f_{7/2}$-shell nuclei will be presented in the order of increasing A: ^{42}Sc, ^{43}Sc, ^{44}Ca, ^{48}Ti, ^{49}V, ^{50}Cr, ^{51}Mn, ^{52}Cr, ^{53}Mn, and ^{54}Fe. Preliminary reports of most of these experimental results have previously been made.[10-12] An extensive study[13] in ^{48}V will be published separately. Referencing for each nucleus will be limited to recent general references for identification of level structure, spin and parity assignments, and γ-decay properties, and to other references pertaining to previous lifetime measurements. The γ-ray spectra for each level studied are shown for three representative plunger distances. The computer fit to these spectra, which were discussed in Sec. II, are represented by solid and dashed curves. All of the obtained ratio data $R - R_\infty$ are plotted as a function of the plunger distance for each case. Unless otherwise stated the solid curves through the ratio data are the best fits to Eq. (1). The resulting lifetimes in-

TABLE I. Lifetime results.

Nucleus	J^π	energy (keV)	τ (psec)
^{42}Sc	3^+	1491	45^{+10}_{-7}
	5^+	1511	57 ± 10
^{43}Sc	$\frac{15}{2}^-$	2987	8.1 ± 1.1
^{44}Ca	6^+	3285	19.6 ± 1.7
^{48}Ti	6^+	3334	12.8 ± 1.2
	$(6)^+$	3507	<3.5
^{49}V	$\frac{11}{2}^-$	1021	5.1 ± 1.0
	$\frac{15}{2}^-$	2261	<3.5
^{50}Cr	2^+	783	12.6 ± 2.1
	4^+	1881	<4.1
	6^+	2164	<2.3
	$\geq 4^+$	3825	<2.0
^{51}Mn	$\frac{7}{2}^-$	238	20.4 ± 3.3
^{52}Cr	4_1^+	2369	$13.7^{+3.6}_{-2.3}$
	6^+	3114	59.5 ± 3.3
	$(3^\pm, 5^-)$	3469	10.4 ± 1.2
	4_2^+	2766	<10
	5^+	3617	<5.5
^{53}Mn	$\frac{13}{2}^-$	2563	15.5 ± 1.8
	$\frac{15}{2}^-$	2693	3.9 ± 0.6
	$\frac{17}{2}^-$	3440	<1.7
^{54}Fe	4^+	2538	5.7 ± 1.2
^{18}F	3^+	937	68.3 ± 3.1

cluding the corrections of Sec. II and the uncertainties will be given for each measurement; all final lifetime values are collected as a summary in Table I.

^{42}Sc

In ^{42}Sc, the lifetimes of the 1491-keV 3^+ and 1511-keV 5^+ levels have been measured by studying the 880-keV transition to the 611-keV 1^+ level and the 894-keV transition to the 617-keV 7^+ level, respectively. The ^{42}Sc decay scheme shown in Fig. 2 for levels below 2.3 MeV is based on Refs. 14–17. Previous lifetime information has been obtained for several levels in ^{42}Sc with the DSAM[14,16] Results from a recent plunger measurement are also available.[18] Because of the difficulty of isolating the 3^+ and 5^+ levels from delayed cascade γ transitions, the plunger measurements were made with both the ^{39}K(α,n)^{42}Sc and ^{40}Ca(^{3}He,p)^{42}Sc reactions at several bombarding energies to ensure reliability.

The final ^{39}K(α,n)^{42}Sc plunger results were obtained with a 140-μg/cm^2 natural KI target at an effective $E_\alpha = 10.04$ MeV which for threshold reasons eliminated the possibility of cascade feeding to the 3^+ and 5^+ levels. This energy, which resulted from a bombarding energy of 10.40 MeV and a 360-keV energy loss in the 2.2-μg/cm^2 Au backing, populated levels in ^{42}Sc only up to an excitation of 1770 keV. Unfortunately, at this low energy, the γ rays of interest are very weak compared to background. Thus, to achieve greater sensitivity to these γ rays, a background spectrum taken at a larger plunger distance and at $E_\alpha = 9.7$ MeV, which is below the threshold for both the 3^+ and 5^+ levels, was subtracted from each plunger spectra after normalization. An unsubtracted spectrum is shown in the top left of Fig. 3. The large peak in this spectrum is the shifted peak of the 899-keV γ ray in ^{42}Ca from the ^{39}K(α,p)^{42}Ca reaction which is not observed to have a stopped peak except at the closest plunger distance. The resulting plunger spectra are shown in the lower left of Fig. 3. To be certain that the 875- and 889-keV γ rays from ^{42}Ca[19] did not interfere with the 880- and 894-keV γ rays from ^{42}Sc, only the shifted and unshifted peaks, respectively, of each transition, normalized to the shifted peak of the 899-keV γ ray, were used to obtain decay ratios. These ratios shown in Fig. 4 were fitted with the decay curve of Eq. (2); a correction for the velocity distribution is small in this case compared to the experimental error. Mean lifetimes $\tau = 47 \pm 13$ psec for the 3^+ level and $\tau = 52 \pm 14$ psec for the 5^+ level were obtained. In addition, the 611-keV $1^+ \rightarrow$ ground-state 0^+ transition yielded an apparent $\tau = 41 \pm 18$ psec due to the feeding from the 3^+ level (the mean life of this 1^+ level has been measured[14] to be $\tau = 0.04$ psec).

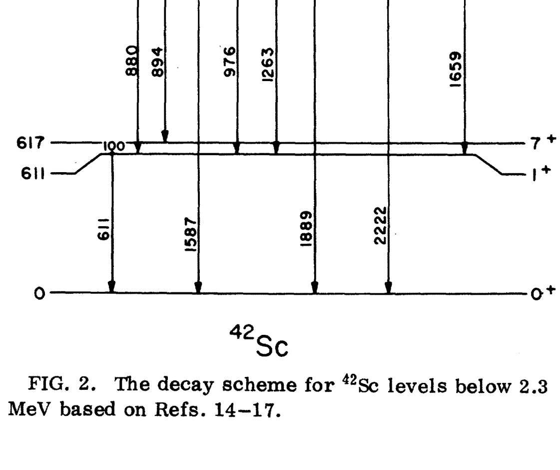

FIG. 2. The decay scheme for ^{42}Sc levels below 2.3 MeV based on Refs. 14–17.

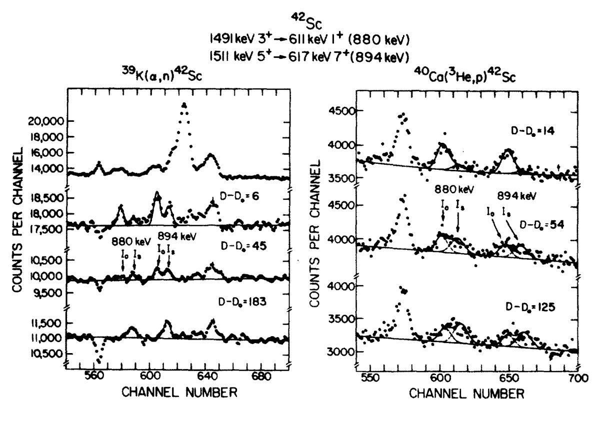

FIG. 3. Recoil-distance γ-ray spectra for the ^{42}Sc 1491-keV $3^+ \rightarrow$ 611-keV 1^+ (880-keV) transition and the 1511-keV $5^+ \rightarrow$ 617-keV 7^+ (894-keV) transition. The left-hand portion displays the spectra obtained from the ^{39}K(α,n)^{42}Sc reaction. The top two spectra show the region of interest obtained with $E_\alpha = 10.4$ MeV at $D - D_0 = 6$ μm before and after the subtraction of a background spectrum obtained with a beam energy below the threshold for the 1491-keV level in ^{42}Sc ($E_\alpha = 9.7$ MeV). Subtracted spectra at two other plunger distances, $D - D_0$ in μm, are shown at the bottom left-hand portion. A constant background has also been added to these subtracted spectra. The right-hand portion displays the spectra from the ^{40}Ca(^{3}He,p)^{42}Sc reaction at three plunger distances.

Initial $^{39}K(\alpha, n)^{42}Sc$ plunger measurements were made with a 14.5-MeV bombarding energy which populated levels up to about 5 MeV excitation. The plunger spectra at this energy contained two additional γ rays, 810 and 917 keV, which showed observable lifetimes, but which could not be fitted into the previously known level scheme. The concern over cascade feeding of the 3^+ and 5^+ levels from such transitions put the preliminary data[10] at this energy in doubt.

The $^{40}Ca(^3He, p)^{42}Sc$ reaction which populates the 3^+ and 5^+ levels with fair strength was used for additional plunger measurements on these levels to achieve improved statistical accuracies with different γ-ray background conditions. The 810- and 917-keV γ rays mentioned above were not observed with this reaction. The kinematics for this reaction at a bombarding energy of 10.5 MeV allowed large recoil angles which resulted in a correspondingly large spread in recoil velocities; hence, in this case the finite target thickness (50-$\mu g/cm^2$ natural Ca on a Au backing) produced a measurable background R_∞ due to a small fraction of the ions stopping in the target.

The plunger results for the 3^+ and 5^+ levels obtained with the ($^3He, p$) reaction are shown in Figs. 3 and 5. Mean lifetimes $\tau = 44^{+24}_{-9}$ psec for the 3^+ level and $\tau = 62 \pm 11$ psec for the 5^+ level were obtained. The asymmetric error bar in the former case is due to the fact that the shifted peak of the 871-keV γ ray from the $\tau = 260$ psec $\frac{1}{2}^+$ level in ^{17}O obscures the 880-keV γ ray in ^{42}Sc at large plunger distances which introduces an uncertainty in R_∞. The 976-keV γ ray from the 1587-keV $2^+ \to 611$-keV 1^+ transition in ^{42}Sc was observed to have a small component which yielded a mean lifetime of 61 ± 18 psec that could be due to feeding from the 1846-keV (3^+) level (the mean lifetime of the 1587-keV 2^+ level has been measured[14] to be $\tau = 0.1$ psec).

Several contaminant γ rays appeared in the spectrum due to partial oxidation of the Ca target. Among them the 937-keV $3^+ \to$ ground-state 1^+ transition in ^{18}F from the $^{16}O(^3He, p)^{18}F$ reaction yielded an improved mean lifetime $\tau = 68.3 \pm 3.1$ psec for the 3^+ level in ^{18}F, in good agreement with a previous measurement[20] of 68 ± 7 psec.

The adopted ^{42}Sc mean lifetimes from the present measurements with both reactions are $\tau = 45^{+10}_{-7}$ psec for the 1491-keV 3^+ level and $\tau = 57 \pm 11$ psec for the 1511-keV 5^+ level. It is interesting to compare these results with those of Bertin, Kumbartzki, and Hirko[18] who measured $\tau = 45 \pm 7$ psec and 74 ± 11 psec for the 3^+ and 5^+ ^{42}Sc levels, respectively, using a n-γ coincidence recoil-distance measurement with the $^{39}K(\alpha, n)^{42}Sc$ reaction at $E_\alpha = 14$ MeV. Although their 3^+ lifetime agrees with the present measurements, their 5^+ lifetime is in slight disagreement and is essentially equal to the preliminary decay slope deduced from the present $^{39}K(\alpha, n)^{42}Sc$ singles measurement at $E_\alpha = 14.5$ MeV that contained the feeding difficulties. Hence, this n-γ coincidence measurement[18] has the same feeding concern, since the proton-recoil spectrum of the neutron detector does not easily isolate these levels from cascade feeding.

^{43}Sc

In ^{43}Sc, the lifetime of the 2987-keV $\frac{15}{2}^-$ level has been measured via the 1157-keV $\frac{15}{2}^- \to \frac{11}{2}^-$ transition. This level, along with the 3123-keV

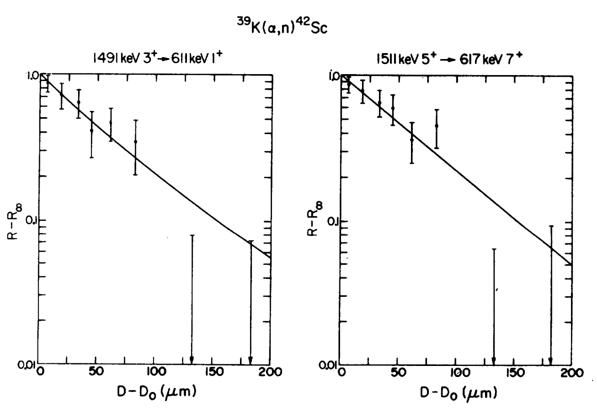

FIG. 4. Lifetime decay plots for the ^{42}Sc 1491-keV $3^+ \to 611$-keV 1^+ and 1511-keV $5^+ \to 617$-keV 7^+ transitions obtained from the $^{39}K(\alpha, n)^{42}Sc$ reaction. The curves through the data points, which have been normalized to 1.0 at $D - D_0 = 0$, represent a least-squares fit of Eq. (2) to the data.

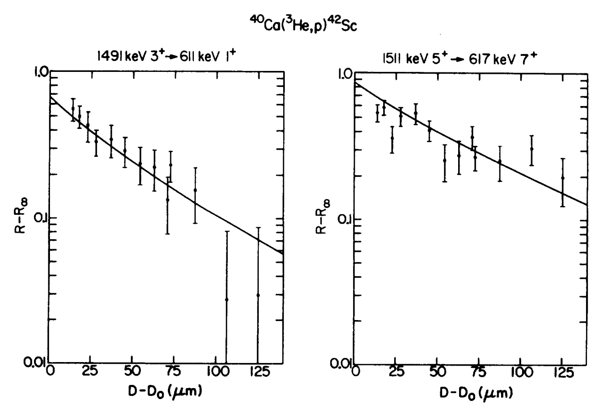

FIG. 5. Lifetime decay plots for the ^{42}Sc 1491-keV $3^+ \to 611$-keV 1^+ and 1511-keV $5^+ \to 617$-keV 7^+ transitions obtained from the $^{40}Ca(^3He, p)^{42}Sc$ reaction. The curves through the data points represent a least-squares fit of Eq. (1) to the data.

$\frac{19}{2}^-$ level, has recently been identified using the $^{40}Ca(\alpha,p)^{43}Sc$ reaction.[21] The low-lying level scheme of ^{43}Sc has been well studied.[22] Extensive lifetime measurements have been made previously for many low-lying levels by the DSAM,[23–25] the recoil-distance,[26,27] and electronic timing techniques.[21] For the present measurement, the $^{40}Ca(\alpha,p)^{43}Sc$ reaction with $E_\alpha = 14.0$ MeV was used to excite the 2987-keV $\frac{15}{2}^-$ level. The target consisted of 48 $\mu g/cm^2$ of natural Ca metal evaporated onto the Au backing. The plunger results for the 1157-keV transition from the $\frac{15}{2}^-$ level to the 1830-keV $\frac{11}{2}^-$ level are shown in Fig. 1. Since the $\frac{15}{2}^-$ level is fed to a small extent by the $\tau = 650$ nsec, $\frac{19}{2}^-$ level, a stopped peak I_0 was observed at large plunger distances; this caused no difficulty in the lifetime determination since the constant contribution is contained in the background R_∞. The resulting mean life for the $\frac{15}{2}^-$ level at 2987 keV in ^{43}Sc is $\tau = 8.1 \pm 1$ psec. Many other transitions were observed between states of lower excitation energy and lower spin; however, no lifetimes for these levels were obtained in the present experiment because of feeding effects from higher transitions.

Because of the natural Ca target, a contamination near the 1157-keV peak was possible due to the γ decay of the 2^+ level in ^{44}Ca at 1155 keV that could be produced by inelastic excitation of the naturally abundant (2.1%) ^{44}Ca. A γ-ray measurement on a ^{44}Ca isotopically enriched (98.5%) target at the same α-beam energy showed that the 1155-keV γ ray had a negligible effect (<5%) on the ^{43}Sc measurement.

^{44}Ca

The lifetime of the 6^+ level in ^{44}Ca at 3285 keV was measured observing the 1002-keV γ-ray transition from the 3285-keV 6^+ level to the 2283-keV 4^+ level. Recent level-scheme information for ^{44}Ca is given in Refs. 28 and 29. Previous lifetime measurements in this nucleus utilized the DSAM.[30]

For the present measurements, the excited ^{44}Ca nuclei were produced by the $^{41}K(\alpha,p)^{44}Ca$ reaction with $E_\alpha = 14.0$ MeV using a 80-$\mu g/cm^2$ KI target isotopically enriched to ~99% ^{41}K. The results for the 1002-keV $6^+ \to 4^+$ transition are shown in Fig. 6. The mean lifetime obtained for the 6^+ level at 3285 keV in ^{44}Ca is $\tau = 19.6 \pm 1.7$ psec. No feeding difficulties were observed from the γ-ray transitions known to cascade to the 6^+ level.[29] The lowest 8^+ level of the $(f_{7/2})^4$ configuration is not expected to affect this lifetime measurement even if populated because of its high excitation energy and thus short lifetime.

^{48}Ti

The lifetime of the 6^+ level in ^{48}Ti at 3334 keV was measured by observing the 1038-keV transition from the 6^+ level to the 4^+ level at 2296 keV. An upper limit has also been obtained for the lifetime of the 3507 keV $(6)^+$ level. References 31 and 32 give a summary of the low-lying level scheme. Lifetimes of a number of levels of ^{48}Ti have been measured by the DSAM.[33]

In the present measurement the 6^+ level was populated with the $^{45}Sc(\alpha,p)^{48}Ti$ reaction at $E_\alpha = 10$ MeV using a 70-$\mu g/cm^2$ natural Sc target. The plunger results for the $6^+ \to 4^+$ transition are shown in Fig. 7. The mean lifetime deduced for the 6^+ level at 3334 keV in ^{48}Ti is $\tau = 12.8 \pm 1.2$ psec. The branch from the 3507-keV $(6)^+$ level that feeds the 3334-keV 6^+ level[32] was observed with an intensity of about 25% that of $6^+ \to 4^+$ transition. An upper limit (2σ) of $\tau < 3.5$ psec was placed on the mean lifetime of this 3507-keV level from the observation that the branch to the 2296-keV 4^+ level showed no appreciable stopped peak at the smallest plunger distance.

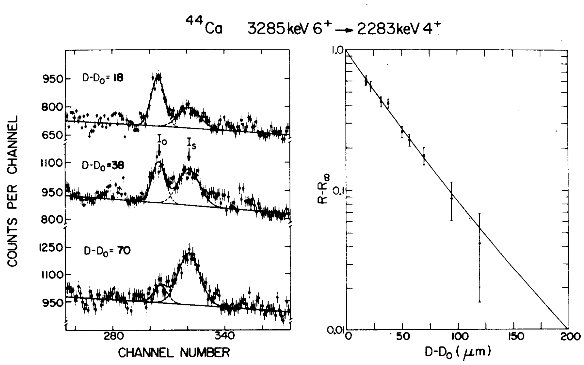

FIG. 6. Recoil-distance γ-ray spectra and lifetime decay curve for the ^{44}Ca 3285-keV $6^+ \to 2283$-keV 4^+ transition. The presentation is similar to that of Fig. 1.

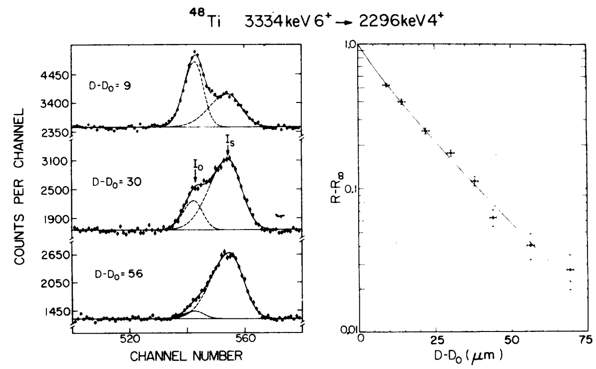

FIG. 7. Recoil-distance γ-ray spectra and lifetime decay curve for the ^{48}Ti 3334-keV $6^+ \to 2296$-keV 4^+ transition. The presentation is similar to that of Fig. 1.

^{49}V

In ^{49}V, the lifetime of the 1021-keV $\frac{11}{2}^-$ level has been measured and an upper limit has been obtained for the lifetime of the 2261-keV $\frac{15}{2}^-$ level. Low-lying levels of ^{49}V are described in Refs. 34, 35, and 36. Lifetimes for the first two excited levels are well known[34,37] and the DSAM has recently been used to measure lifetimes of numerous levels up to 2.5 MeV excitation energy.[38,39]

The ^{46}Ti$(\alpha, p)^{49}$V reaction with $E_\alpha = 11.0$ MeV has been used to excite the 1021-keV $\frac{11}{2}^-$ level. The target consisted of 60 μg/cm^2 of ^{46}Ti isotopically enriched to 80%. The plunger results for the 1021-keV $\frac{11}{2}^- \to \frac{7}{2}^-$ ground-state transition are shown in Fig. 8. The mean lifetime obtained for the 1021-keV $\frac{11}{2}^-$ level in ^{49}V is $\tau = 5.1 \pm 1.0$ psec. This value is in agreement with a recent DSAM lower limit of $\tau > 3.4$ psec.[38] Two γ rays which have been previously reported to feed the $\frac{11}{2}^-$ level with energies of 134 keV[34] and 1330 keV[36] were not observed with this reaction.

The 1240-keV γ ray from the 2261-keV $\frac{15}{2}^- \to$ 1021-keV $\frac{11}{2}^-$ transition[35] is observed in the present experiment with an intensity at 0° of approximately $\frac{1}{6}$ the intensity of the 1021-keV γ ray. Using this transition, an upper limit (2σ) of $\tau < 3.5$ psec was obtained for the mean lifetime of the 2261-keV $\frac{15}{2}^-$ level. The weak feeding from this level does not affect the lifetime for the 1021-keV $\frac{11}{2}^-$ level.

^{50}Cr

In ^{50}Cr, the lifetime of the first excited 783-keV 2^+ level and lifetime limits for several higher excited levels have been measured. The level scheme in Fig. 9 showing only the transitions discussed here is taken from Refs. 40 and 41. Previously measured lifetimes in ^{50}Cr have been obtained with the DSAM[40,42] and the plunger method.[41]

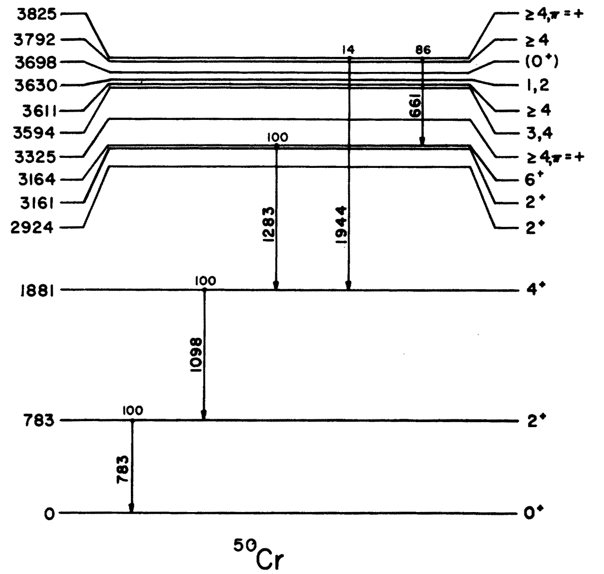

FIG. 9. The decay scheme for ^{50}Cr based on Refs. 40 and 41. Only the transitions discussed in the text are shown.

In the present experiment the levels of interest were populated by the ^{40}Ca$(^{16}$O$, \alpha 2p)^{50}$Cr reaction with an ^{16}O beam of 47 MeV using a 260-μg/cm^2 natural Ca metal target. The bombardment of the ^{40}Ca target with ^{16}O strongly populated many high-spin states in ^{54}Fe, ^{53}Fe, ^{53}Mn, ^{51}Mn, and ^{50}Cr. Recoil-distance lifetimes were obtained for ^{54}Fe, ^{53}Mn, and ^{51}Mn levels in addition to those in ^{50}Cr.

The plunger results for the 783-keV 2^+ levels in ^{50}Cr are shown in Fig. 10. A mean lifetime of $\tau = 12.6 \pm 2.1$ psec for this 2^+ level was obtained. All strong transitions which are shown to feed this

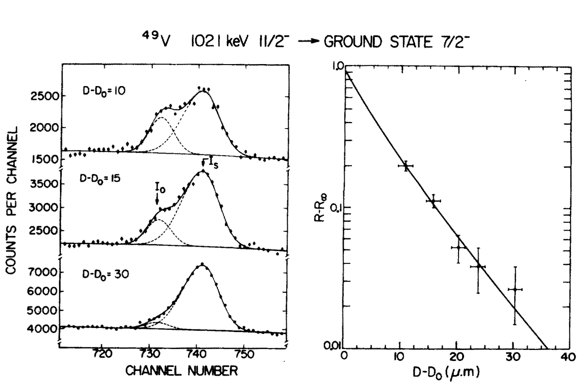

FIG. 8. Recoil-distance γ-ray spectra and lifetime decay curve for the ^{49}V 1021-keV $\frac{11}{2}^- \to$ ground-state $\frac{7}{2}^-$ transition. The presentation is similar to that of Fig. 1.

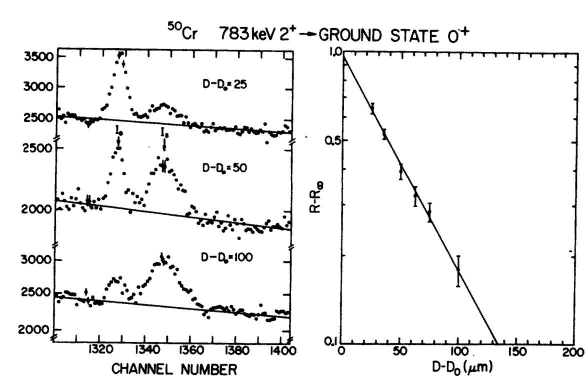

FIG. 10. Recoil-distance γ-ray spectra and lifetime decay curve for the ^{50}Cr 783-keV $2^+ \to$ ground-state 0^+ transition. The presentation is similar to that of Fig. 1.

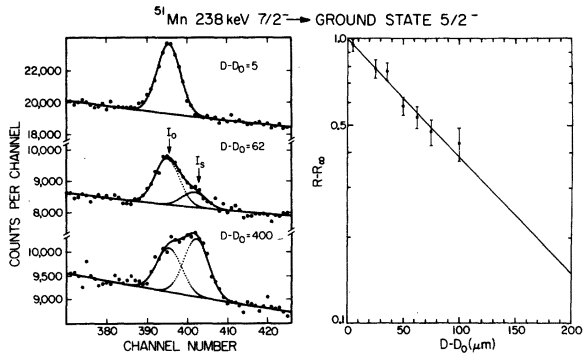

FIG. 11. Recoil-distance γ-ray spectra and lifetime decay curve for the ^{51}Mn 238-keV $\frac{7}{2}^- \rightarrow$ground-state $\frac{5}{2}^-$ transition. The presentation is similar to that of Fig. 1.

level indicated considerably shorter lifetimes. From the observation of the feeding transitions shown in Fig. 9, mean-lifetime upper limits (2σ) of 4.1, 2.3, and 2.0 psec were obtained for the 1881-keV 4^+, 3164-keV 6^+, and 3825-keV ($J \geq 4^+$) levels, respectively. The present lifetime obtained for the 783-keV 2^+ level is in good agreement with previous measurements of $\tau = 10 \pm 2$ psec from the DSAM and $\tau = 12.1 \pm 1.2$ psec from Coulomb excitation.[40] Recently, other plunger lifetime measurements for ^{50}Cr have been reported by Dehnhardt *et al.*[41] Their lifetime results of 12.1 ± 1.2, 3.2 ± 0.4, and 1.8 ± 0.4 psec for the 783-keV 2^+, 1881-keV 4^+ and 2164-keV 6^+ levels, respectively, are in agreement with the present results.

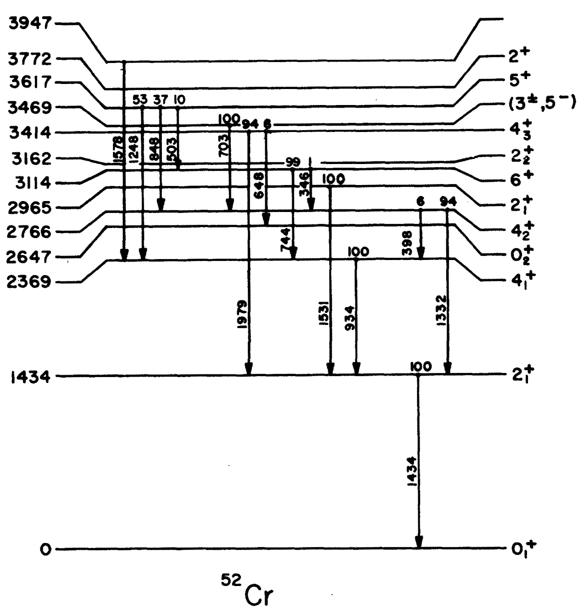

FIG. 12. The decay scheme for ^{52}Cr levels below 4 MeV based on Ref. 45. Only the transitions discussed in the text are shown.

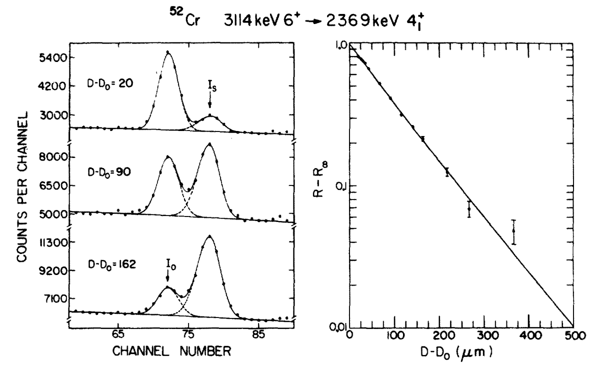

FIG. 13. Recoil-distance γ-ray spectra and lifetime decay curve for the ^{52}Cr 3114-keV $6^+ \rightarrow$ 2369-keV 4_1^+ transition. The presentation is similar to that of Fig. 1.

^{51}Mn

In ^{51}Mn, the lifetimes of the first excited 238-keV $\frac{7}{2}^-$ level has been measured using the ^{40}Ca-(^{16}O, αp)^{51}Mn reaction with an ^{16}O beam of 47 MeV using a 260-μg/cm^2 natural Ca metal target. Recently, the decay scheme from the (p, γ) reaction has been reported[43] and lifetimes have been measured with the DSAM.[44]

The plunger results for the 238-keV $\frac{7}{2}^- \rightarrow \frac{5}{2}^-$ ground-state transition are shown in Fig. 11. The mean lifetime obtained for the 238-keV $\frac{7}{2}^-$ level in ^{51}Mn is $\tau = 20.4 \pm 3.3$ psec. Several transitions which are known to feed the $\frac{7}{2}^-$ level[44] did not show plunger lifetimes. The 238-keV γ ray showed a 40% stopped peak even at large distances ($D - D_0 \approx 2500$ μm). If this is not due to a contaminant γ-ray, it perhaps originates from a level in ^{51}Mn with a mean life $\tau \gtrsim 1$ nsec or from the β decay of ^{51}Fe. Neither situation would affect the lifetime result.

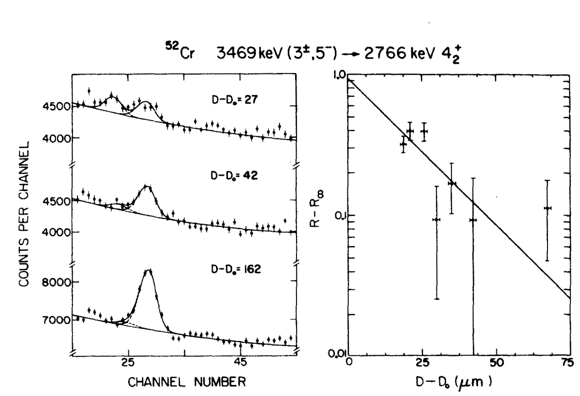

FIG. 14. Recoil-distance γ-ray spectra and lifetime decay curve for the ^{52}Cr 3469-keV ($3^{\pm}$,5^-) $\rightarrow$ 2766-keV 4_2^+ transition. The presentation is similar to that of Fig. 1.

^{52}Cr

In ^{52}Cr, the lifetimes for the 2369-keV 4_1^+, 3114-keV 6^+, and 3469-keV $(3^\pm, 5^-)$ levels and lifetime limits for the 2677-keV 4_2^+ and the 3617-keV 5^+ levels were obtained. The level scheme for levels below 4 MeV in Fig. 12 showing only the transitions to be discussed is based on Ref. 45. Previous lifetime measurements have been made with the DSAM.[42,45]

In the present experiment, levels in ^{52}Cr were populated with the ^{49}Ti$(\alpha, n)^{52}$Cr reaction with $E_\alpha = 14.5$ MeV using a 30-μg/cm^2 Ti metal target isotopically enriched to ~80% ^{49}Ti. The decay curves for the 744- and 703-keV transitions from the 6^+ and $(3^\pm, 5^-)$ levels, respectively, are shown in Figs. 13 and 14. Mean lifetimes of $\tau = 59.5 \pm 3.3$ psec for the 3114-keV 6^+ level and $\tau = 10.4 \pm 1.2$ psec for the 3469-keV $(3^\pm, 5^-)$ level were obtained. Since the 2369-keV 4_1^+ level is strongly fed by the 744-keV transition from the 6^+ level, the lifetime of the 4_1^+ level was obtained by fitting the experimental ratios for the 934-keV $4_1^+ \rightarrow 2_1^+$ transition to Eq. (3) which explicitly takes into account the feeding from the 6^+ level whose lifetime was fixed at the above measured value. The experimental ratios, $R - R_\infty$, are shown in Fig. 15 with the solid curve representing the best fit to Eq. (4). The experimental ratios and best fit are also shown in the same figure after the feeding component $Af'\tau' e^{-(D-D_0)/\bar{v}\tau'}/(\tau' - \tau)$, has been subtracted [see Eq. (4)]. The mean lifetime obtained for the 2369-keV 4_1^+ level was $13.7^{+3.6}_{-2.3}$ psec.

An upper limit (2σ) of $\tau < 5.5$ psec for the 3617-keV 5^+ level was obtained from the observation of the 1248-keV γ ray which originates from this level. Thus the γ-ray branches for this level to the 4_1^+ and 6^+ levels, which were weak in the spectra, did not present feeding problems. An upper limit (2σ) of $\tau < 10$ psec was obtained for the 2766-keV 4_2^+ level by observing the 1332-keV decay γ ray. The 398-keV transition from this 4_2^+ level to the 4_1^+ level was too weak to present feeding problems. A preliminary result reported for the 2766-keV 4_2^+ level[11] is in doubt because of partial feeding from the 3469-keV $(3^\pm, 5^-)$ level. A number of other transitions are known to feed the levels for which plunger lifetimes were obtained; however, they are weak in the spectra and originate from levels whose lifetimes are less than 2 psec.[45]

Most of the plunger lifetimes agree with those obtained from the measurements of Sprague *et al.*[45] Mean lifetime limits of $1.1 < \tau < 5.5$ psec can be obtained for the 3617-keV 5^+ level by combining the present result with the DSAM value of $\tau > 1.1$ psec. However, the DSAM measurement of $\tau = 1.5^{+0.50}_{-0.25}$ psec for the 2369-keV 4_1^+ level[45] is in disagreement with the present recoil-distance result of $\tau = 13.7^{+3.6}_{-2.3}$ psec. This DSAM measurement was done in singles so that the observed centroid shift has to be corrected for feeding from the 6^+ whose lifetime was not known. The present result which explicitly takes into account the 6^+ feeding should be more reliable.

^{53}Mn

In ^{53}Mn, the lifetimes of the 2693-keV $\frac{15}{2}^-$ and the 2563-keV $\frac{13}{2}^-$ levels have been measured and

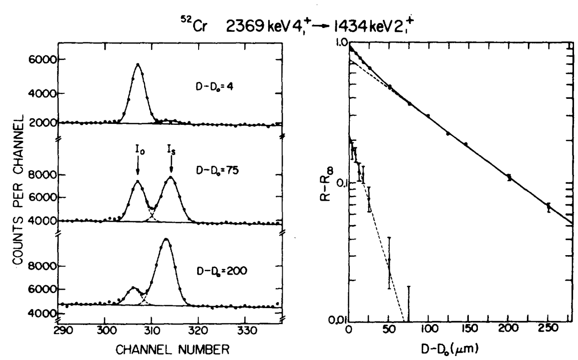

FIG. 15. Recoil-distance γ-ray spectra and lifetime decay curve for the ^{52}Cr 2369-keV $4_1^+ \rightarrow 1434$-keV 2_1^+ transition. The presentation is similar to that of Fig. 1 except that the ratio data were fit using Eq. (4) to take into account the feeding from the 3114-keV 6^+ level. The lifetime decay plot and fitted curve are also shown with the feeding component subtracted.

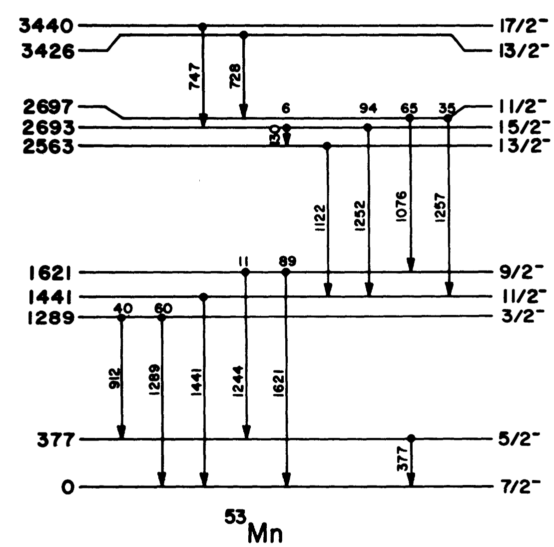

FIG. 16. The decay scheme for high-spin states in ^{53}Mn taken from Ref. 46.

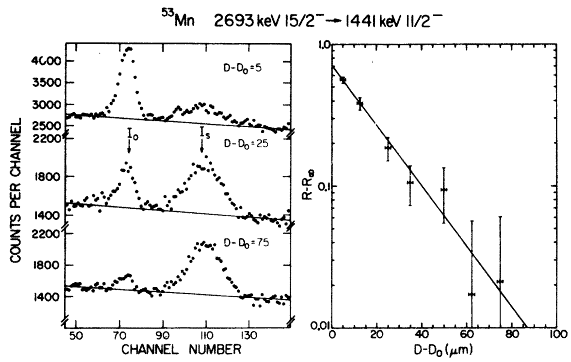

FIG. 17. Recoil-distance γ-ray spectra and lifetime decay curve for the ^{53}Mn 2693-keV $\frac{15}{2}^-$ → 1441-keV $\frac{11}{2}^-$ transition. The presentation is similar to that of Fig. 1.

an upper limit has been obtained for the lifetime of the 3440-keV $\frac{17}{2}^-$ level. The level scheme in Fig. 16 showing the high-spin levels in ^{53}Mn is based on the work of Sawa *et al.*[46] The DSAM[47,48] and the electronic timing method[49] have been used previously to measure several ^{53}Mn lifetimes.

In the present experiment, levels in ^{53}Mn were populated using the ^{40}Ca(^{16}O, $3p$)^{53}Mn reaction with an ^{16}O beam of 47 MeV using a 260-μg/cm^2 natural Ca metal target. Only the transitions among the highest-spin states in ^{53}Mn, 3440-keV $\frac{17}{2}^-$, 2693-keV $\frac{15}{2}^-$, 2564-keV $\frac{13}{2}^-$, 1441-keV $\frac{11}{2}^-$, and ground-state $\frac{7}{2}^-$, were observed (the 377-keV $\frac{5}{2}^-$ level was populated by the β^+ decay of ^{53}Fe). The decay curve for the 1252-keV transition from the 2693-keV $\frac{15}{2}^-$ level shown in Fig. 17 yielded a mean lifetime of $\tau = 3.88 \pm 0.55$ psec for the $\frac{15}{2}^-$ level. An upper limit (2σ) of $\tau < 1.7$ psec was obtained for the lifetime of the 3440-keV $\frac{17}{2}^-$ level by observing the 747-keV γ ray, which feeds the 2693-keV $\frac{15}{2}^-$ level.

The γ-ray spectra for the 1122-keV transition from the 2563-keV $\frac{13}{2}^-$ level to the 1441-keV $\frac{11}{2}^-$ level are shown in Fig. 18 and the ratio data are shown in Fig. 19. A mean lifetime of $\tau = 15.5 \pm 1.8$ psec was obtained for the 2563-keV $\frac{13}{2}^-$ level. Using the $E2/M1$ mixing ratio of $\delta = -0.02 \pm 0.02$ obtained by Sawa *et al.* for the $\frac{13}{2}^- \to \frac{11}{2}^-$ transition,[46] a $B(M1) = [(26 \pm 3) \times 10^{-4}]\mu_N{}^2$ and a $B(E2) \leq 0.052$ e^2 fm^4 were obtained. Although the $\frac{13}{2}^-$ level is not part of the $(f_{7/2})^{-3}$ configuration, the hindrance of the $M1$ strength is comparable to that obtained for several transitions in ^{51}V for $(f_{7/2})^3$ levels. The $E2$ hindrance for this transition suggests that this $\frac{13}{2}^-$ level consists of a neutron core excitation.

^{54}Fe

The lifetime of the 2538-keV 4^+ level in ^{54}Fe was measured using the ^{40}Ca(^{16}O, $2p$)^{54}Fe reaction with an ^{16}O beam of 47 MeV and a 260 μg/cm^2 natural Ca target. Previously, the lifetime of the 2950-keV 6^+ state has been measured by electronic timing.[50,51]

The γ-ray spectra for the 1130-keV transition from the 2583-keV 4^+ level to the 1408-keV 2^+ level are shown in Fig. 18. The 4^+ level is primarily fed indirectly from the 6^+ level which has a mean lifetime of 1749 ± 23 psec[50,51]; this feeding gives a stopped peak even at large plunger distances. Since the shifted peak was obscured by the ^{53}Mn 1122-keV shifted peak, the ratios R were

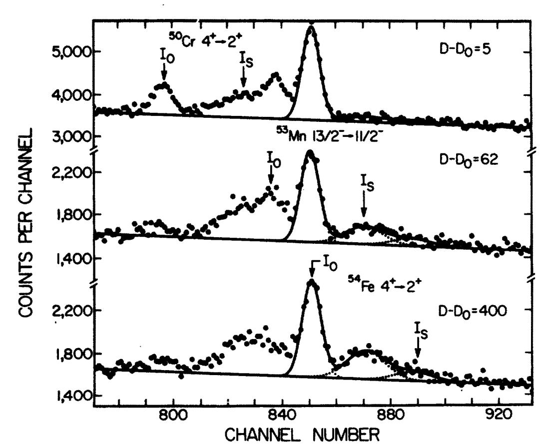

FIG. 18. Recoil-distance γ-ray spectra for a region of interest from the bombardment of ^{40}Ca with a 47-MeV ^{16}O beam taken at three different plunger distances, $D - D_0$ in μm. The unshifted and shifted peaks, I_0 and I_S, are indicated for the ^{50}Cr $4^+ \to 2^+$, ^{53}Mn $\frac{13}{2}^- \to \frac{11}{2}^-$, and ^{54}Fe $4^+ \to 2^+$ transitions.

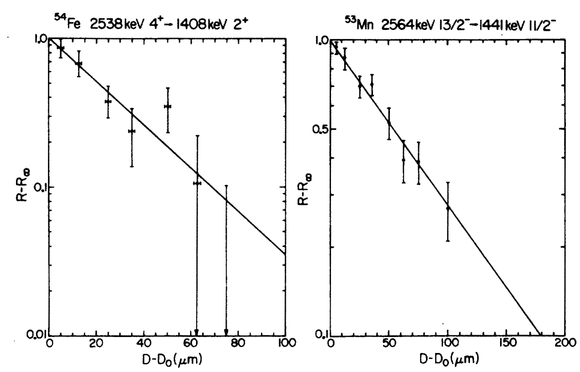

FIG. 19. Lifetime decay curves for the ^{54}Fe 2538-keV 4^+→1408-keV 2^+ and ^{53}Mn 2564-keV → $\frac{13}{2}^-$ 1441-keV $\frac{11}{2}^-$ transitions. The ratio data for the ^{54}Fe transition were obtained by normalizing the unshifted peak I_0 to the 547-keV γ ray produced by Coulomb excitation of the Au target backing and plunger. The data points for the ^{53}Mn transition were obtained by normalizing the shifted peak I_S also to the 547-keV γ ray. The curves through the data points represent fits using Eq. (2).

obtained by normalizing the 1130-keV unshifted peak to the 547-keV γ ray produced by Coulomb excitation from the Au target backing and stopper. These ratios, after background subtraction and with a normalization to 1.0 at $D-D_0=0$, are shown in Fig. 19 with a straight-line fit using Eq. (2). A mean lifetime of $\tau=5.7\pm1.2$ psec was obtained for the 2538-keV 4^+ level.

IV. DISCUSSION

The lifetimes obtained for nuclei with $40<A<56$ from the present recoil-distance measurements together with those obtained previously by other methods provide a rather complete set of $E2$ transition probabilities among levels which can be described to a large extent by the $(1f_{7/2})^n$ configuration. In this section, the success of the effective operator approach towards an explanation of these $E2$ strengths will be explored.

The $E2$ operator, $O(E2)$, and its connection to the reduced transition probability are defined by the following expressions:

$$O(E2)=\sum_i\left[\tfrac{1}{2}e_n(1+\tau_{zi})+\tfrac{1}{2}e_p(1-\tau_{zi})\right]r_i^2Y_i^{(2)}\,, \tag{5}$$

$$B(E2)=(2J_i+1)^{-1}|\langle\psi_f\|O(E2)\|\psi_i\rangle|^2\,.$$

When the wave functions are limited to a truncated shell-model space in order to make theoretical calculations feasible, the normal "bare" nucleon charges $e_p=e$ and $e_n=0$ are modified into effective charges yielding an effective $E2$ operator.[1] Appropriate wave functions for the nuclear states within the truncated shell-model space are determined from effective two-body matrix elements. The effective charges, e_p and e_n, can be extracted from a comparison of the experimental $B(E2)$ values with those calculated from Eq. (5) for the given set of wave functions.

The difference between the effective charges and the normal bare charges is directly related to the core-polarization contributions provided the truncated wave functions adequately describe the nuclear states. When significant parts of the nuclear states are not included in the truncated space, then the extracted effective charges will incorporate additional contributions. Thus if the extracted effective charges are constant or vary in a consistent manner for many transitions, this effective-operator approach can successfully contribute to an understanding of the nuclear structure even though it may be difficult to isolate the core-polarization contributions. This approach, however, fails for a selected shell-model space, if the extracted effective charges vary drastically for different transitions.

When limiting the wave functions for the $40<A<56$ nuclei to the $1f_{7/2}$ shell-model space, there are three important contributions that must be accounted for by the effective $E2$ operator. These contributions result from particle excitations of $\Delta N=0$ to other members of the $1f$-$2p$ shell, two-particle excitations each of $\Delta N=1$ from the core, and single-particle core excitations of $\Delta N=2$ ($N=2n+l-1$ refers to the major oscillator shells). The $\Delta N=0$ contributions are the particle excitations from the $1f_{7/2}$ orbital to other $1f$-$2p$ orbitals of which the $2p_{3/2}$ is the most important. Contributions from the $\Delta N=1$ two-particle excitations originate from pairs of particles being excited out of the $2s$-$1d$ shell of the core to the $1f$-$2p$ orbitals. These are core-deformed components which can significantly enhance $E2$ transition strengths.[52-54] Pairs of $1d_{3/2}$ holes are known to be important near ^{40}Ca in this regard. The most theoretically interesting contributions to the effective $E2$ operator are the $\Delta N=2$ single-particle excitations from the $2s$-$1d$ to the $3s$-$2d$-$1g$ orbitals and from the $1p$ to the $1f$-$2p$ orbitals.

The total $\Delta N=2$ single-particle contribution is often associated with the core-polarization charges, $\delta e_n^{\rm pol}$ for the neutron and $\delta e_p^{\rm pol}$ for the proton. A number of theoretical calculations of the core-polarization charge for one particle outside a ^{40}Ca core have been carried out.[3,55-57] An interesting aspect of these calculations is that the quantities $\delta e_0^{\rm pol}=\frac{1}{2}(\delta e_n^{\rm pol}+\delta e_p^{\rm pol})$ and $\delta e_1^{\rm pol}=\frac{1}{2}(\delta e_n^{\rm pol}-\delta e_p^{\rm pol})$ are primarily determined by the $J=2$, $T=0$ and $J=2$, $T=1$ giant resonance states, respectively, in ^{40}Ca. Most of these calculations yield a $\delta e_1^{\rm pol}$ which implies that $\delta e_p^{\rm pol}<\delta e_n^{\rm pol}$. Large variations in the value of $\delta e_0^{\rm pol}$ were obtained from the different calculations.

In the following sections, the extracted effective charges will be presented and interpreted in terms of the above contributions. These results for nuclei near ^{40}Ca with $42\leq A\leq44$ will be presented in Sec. IV A and those for nuclei with $48\leq A\leq54$ in Sec. IV B. This separation is appropriate since the nuclei near ^{40}Ca contain considerable deformed components while for the $48\leq A\leq54$ nuclei with a larger number of particles in the $1f_{7/2}$ shell, these excitations are blocked out to a large extent. In addition, calculations for the nuclei near ^{40}Ca are made with wave functions for both the $1f_{7/2}$ shell and the larger $1f$-$2p$ shell while only the $1f_{7/2}$-shell wave functions are used for the nuclei with $48\leq A\leq54$.

In evaluating the effective charges, the experimental $B(E2)$ values are obtained from the lifetime measurements with the following expression:

$$B(E2)_{\exp}[e^2\,\mathrm{fm}^4]=\frac{816}{(E_\gamma[\mathrm{MeV}])^5}\,\frac{b}{\tau[\mathrm{psec}]}\,, \qquad (6)$$

where $b=\lambda(E2)\tau$ is the branching ratio. All of the γ decays in the present measurements involve only pure $E2$ transitions and thus contain no multipole mixing. Where there are several lifetime measurements in the literature, the best values are determined by the usual weighted average, and the quoted errors include both the experimental spread and the individual uncertainties. For DSAM lifetime measurements, a systematic error of 15% was assumed. To obtain the calculated $B(E2)$ values, the radial integrals were in all cases determined from harmonic-oscillator wave functions with an $\hbar\omega=41A^{-1/3}$ MeV that is consistent with electron scattering measurements of $\langle r^2\rangle$.[58] The comparison methods by which the appropriate effective charge values are extracted for a given set of experimental and calculated $B(E2)$ values will be discussed separately for the different regions of nuclei.

A. $42 \leqslant A \leqslant 44$

The extraction of $E2$ effective charges from the present and previous lifetime results for nuclei with $42 \leqslant A \leqslant 44$ will be discussed in this section. This will first be carried out for both the $1f_{7/2}$ and $1f$-$2p$ shell-model spaces under the assumption that $e_n=\delta e$ and $e_p=1+\delta e$. The experimental and calculated $B(E2)$ values and the corresponding effective charges for the various theoretical approaches are collected in Table II.

With the $(1f_{7/2})^n$ shell-model space the $B(E2)$ values are calculated in a straightforward manner from Eq. (5) for ^{42}Ca, ^{42}Sc, ^{42}Ti, and ^{43}Ca. For the more complex nuclei, ^{43}Sc and ^{44}Ti, the $1f_{7/2}$ wave functions of McCullen, Bayman, and Zamick (MBZ)[59] are used. In ^{44}Ca the lowest 2^+ and 4^+ states are assumed to have seniorities 2 and 4, respectively. The resulting effective charges (Table II) for the high-spin states in ^{42}Ca and ^{43}Ca are consistent with $\delta e\approx 0.9$ while the effective charges for the low-spin states are larger ($\delta e \approx 2.0$) which can be explained by the increased importance of core deformed admixtures. The results for ^{42}Sc, however, are not consistent with this picture; in this nucleus the high spin $5^+\rightarrow 7^+$ transition needs a large charge of $\delta e\approx 1.8$. This anomaly is also reflected to a lesser degree in ^{43}Sc and ^{44}Ti. Thus the effective charge concept with a truncation to the $1f_{7/2}$ shell-model space does not appear to be useful in the $42 \leqslant A \leqslant 44$ region except for the pure neutron (Ca) nuclei.

For the larger $1f$-$2p$ shell-model space, the deduced effective charges are no longer dependent on the $\Delta N=0$ excitations since they are included explicitly in the wave functions. The $B(E2)$ values for the $(fp)^n$ configurations (Table II) have been calculated by McGrory and Bhatt,[60] who used wave functions derived from a complete diagonalization of the Kuo-Brown matrix elements[61] assuming that the nucleons are distributed in the $1f_{7/2}$, $2p_{3/2}$, $1f_{5/2}$, and $2p_{1/2}$ shell-model orbitals. An improvement is seen (Table II) in the consistency of the corresponding effective charges for the high-spin states in all of these nuclei. In particular, the effective charge $\delta e\approx 0.7$ obtained for the $6^+\rightarrow 4^+$ transition in ^{42}Ca is reduced only 20% from that obtained with the $(1f_{7/2})^2$ wave functions while the δe for the ^{42}Sc $5^+\rightarrow 7^+$ transition is reduced from approximately 1.8 to 0.3. The effective charges for low-spin states are still enhanced with the exception of the $2^+\rightarrow 0^+$ transition in ^{44}Ti($\delta e\approx 0.5$). There is also a slight trend for δe to be smaller for the more proton-rich nuclei.

Sufficient data exists to distinguish between the effective proton and neutron charges, if the assumption that the effective charge is independent of the specific orbital is made. The variation in the effective charges between the $1f_{7/2}$ and $2p_{3/2}$ orbitals is not large.[3] The graphical procedure described below will be used under this assumption to show the dependence of the various transition strengths on δe_p and δe_n, where $e_n=\delta e_n$ and $e_p=1+\delta e_p$. Calculated values of $[B(E2)]^{1/2}$, which have the form Ae_p+Be_n, are set equal to $|[B(E2)]^{1/2}_{\exp}|$, which is denoted by C. When this equation is rewritten as

$$\frac{B}{C}=-\frac{e_p}{e_n}\frac{A}{C}+\frac{1}{e_n}\,,$$

the points $(A/C,\ B/C)$ plotted on an (x,y) graph should lie on a line which intersects the y axis at $1/e_n$ and the x at $1/e_p$. The results for the $(fp)^n$ calculations are plotted in this way in Fig. 20. The ^{44}Ca transitions have not been included, since the calculated $B(E2)$ values are very sensitive to the seniority mixing of the 2^+ and 4^+ levels (see the discussion on ^{52}Cr in the next section).

The two lines in Fig. 20 represent the best fits first to the ^{42}Ca $6^+\rightarrow 4^+$ and ^{42}Sc $5^+\rightarrow 7^+$ transitions and secondly to the low spin $2^+\rightarrow 0^+$ transitions in the $A=42$ nuclei. The results of these fits in terms of e_p, e_n, $\delta_0=\frac{1}{2}(\delta e_n+\delta e_p)$ and $\delta_1=\frac{1}{2}(\delta e_n-\delta e_p)$ are given in Table III. Results for all other transitions lie between these two lines as seen in Fig. 20. Specifically, the transitions in the $A=43$ nuclei between high-spin states and those between low-spin states show the same trend as the $A=42$ transitions although they are not as extreme. The transitions in ^{44}Ti lie midway between the two

TABLE II. Comparison of experimental and calculated $B(E2)$ values for transitions in nuclei with $42 \leq A \leq 44$. The calculated $B(E2)$ values (harmonic oscillator radial integrals are used with $\hbar\omega = 41A^{-1/3}$) and the resulting effective charges were obtained with wave functions from three different model spaces.

Nucleus	Transition [a]	Experimental $B(E2)_{exp}$ $[e^2\,fm^4]$	Experimental Refs.	$(1f_{7/2})^n$ Wave functions $\lvert[B(E2)_{th}]^{1/2}\rvert$ $[e\,fm^2]$	$(1f_{7/2})^n$ Wave functions δe $[e]$	$(fp)^n$ Wave functions [b] $\lvert[B(E2)_{th}]^{1/2}\rvert$ $[e\,fm^2]$	$(fp)^n$ Wave functions [b] δe $[e]$	$(fp)^2+(fp)^4(sd)^{-2}$ Wave functions [c] $\lvert[B(E2)_{th}]^{1/2}\rvert$ $[e\,fm^2]$	$(fp)^2+(fp)^4(sd)^{-2}$ Wave functions [c] δe $[e]$
^{42}Ca	$6^+ \to 4^+$	6.44 ± 0.19	d,e	$2.93e_n$	0.867 ± 0.014	$3.77e_n$	0.674 ± 0.011	$0.7e_p + 3.8e_n$	0.409 ± 0.009
	$4^+ \to 2^+$	57.5 ± 4.5	f	$4.34e_n$	1.75 ± 0.07	$5.26e_n$	1.44 ± 0.06	$3.2e_p + 5.7e_n$	0.49 ± 0.03
	$2^+ \to 0^+$	81.5 ± 3.0	g	$4.35e_n$	2.08 ± 0.04	$5.22e_n$	1.73 ± 0.03	$2.1e_p + 5.2e_n$	0.95 ± 0.02
^{43}Ca	$\frac{15}{2}^- \to \frac{11}{2}^-$	16.6 ± 0.7	f	$3.96e_n$	1.028 ± 0.022	$5.04e_n$	0.808 ± 0.018		
	$\frac{11}{2}^- \to \frac{7}{2}^-$	55 ± 16	h,i	$4.62e_n$	1.60 ± 0.26	$5.55e_n$	1.33 ± 0.22		
	$\frac{5}{2}^- \to \frac{7}{2}^-$	86.5 ± 7.0	i	$6.86e_n$	1.36 ± 0.06	$8.01e_n$	1.16 ± 0.05		
	$\frac{3}{2}^- \to \frac{7}{2}^-$	65.5 ± 4.5	h,j	$4.06e_n$	2.00 ± 0.07	$5.33e_n$	1.52 ± 0.06		
^{44}Ca	$6^+ \to 4^+$	41.2 ± 3.6	This exp.	$4.89e_n$ [k]	1.31 ± 0.06	$3.9e_n$	1.65 ± 0.07		
	$2^+ \to 0^+$	100 ± 6	g,l	$5.11e_n$ [k]	1.95 ± 0.06	$6.7e_n$	1.49 ± 0.04		
^{42}Sc	$5^+ \to 7^+$	$25.1^{+5.3}_{-3.8}$	This exp.	$1.07(e_p + e_n)$	1.84 ± 0.23	$3.06(e_p + e_n)$	0.32 ± 0.08	$3.1(e_p + e_n)$	0.31 ± 0.08
	$3^+ \to 1^+$	34.4 ± 6.3	This exp.	$2.30(e_p + e_n)$	0.78 ± 0.13	$2.98(e_p + e_n)$	0.49 ± 0.10	$3.3(e_p + e_n)$	0.39 ± 0.09
	$2^+ \to 0^+$	76^{+34}_{-24}	m	$2.17(e_p + e_n)$	1.50 ± 0.46	$2.61(e_p + e_n)$	1.17 ± 0.38	$3.6(e_p + e_n)$	0.71 ± 0.28
^{43}Sc	$\frac{19}{2}^- \to \frac{15}{2}^-$	27.0 ± 0.8	n	$0.56e_p + 2.80e_n$	1.381 ± 0.024	$1.72e_p + 4.38e_n$	0.570 ± 0.013		
	$\frac{15}{2}^- \to \frac{11}{2}^-$	49^{+8}_{-6}	This exp.	$0.77e_p + 3.83e_n$ [o]	1.35 ± 0.11	$2.08e_p + 5.66e_n$	0.64 ± 0.06		
	$\frac{11}{2}^- \to \frac{7}{2}^-$	123^{+22}_{-16}	p	$0.60e_p + 3.00e_n$ [o]	2.92 ± 0.25	$1.88e_p + 5.49e_n$	1.25 ± 0.12		
^{42}Ti	$2^+ \to 0^+$	134^{+30}_{-21}	q,r	$4.35e_p$	1.67 ± 0.28	$5.22e_p$	1.22 ± 0.23	$5.2e_p + 2.1e_n$	0.88 ± 0.16
^{44}Ti	$6^+ \to 4^+$	157 ± 22	s	$3.19(e_p + e_n)$ [o]	1.46 ± 0.14	$5.9(e_p + e_n)$	0.56 ± 0.08		
	$4^+ \to 2^+$	280 ± 60	t	$4.21(e_p + e_n)$ [o]	1.48 ± 0.23	$6.4(e_p + e_n)$	0.80 ± 0.15		
	$2^+ \to 0^+$	157 ± 22	t	$3.71(e_p + e_n)$ [o]	0.98 ± 0.20	$5.4(e_p + e_n)$	0.52 ± 0.14		

[a] J_i and J_f refer to states of lowest energy with the respective spins.

[b] Reference 60.

[c] Reference 53.

TABLE II (*Continued*)

[d] Reference 50.
[e] R. A. Mendelson and R. T. Carpenter, Phys. Rev. 181, 1552 (1969); L. E. Carlson and A. J. Robertson, private communication quoted in Ref. 53.
[f] A. R. Poletti, B. A. Brown, D. B. Fossan, E. K. Warburton, P. Gorodetsky, J. J. Kolata, and J. W. Olness, to be published.
[g] Reference 54.
[h] Reference 29.
[i] R. N. Horosko, C. Towsley, and D. Cline, in *Proceedings of the Topical Conference on the Structure of* $1f_{7/2}$ *Nuclei* (see Ref. 67), p. 419.
[j] C. Chasman, K. W. Jones, and R. A. Ristinen, Phys. Rev. 169, 911 (1968); H. Gruppelaar, A. M. F. Opdenkamp, and A. M. J. Spits, Nucl. Phys. A131, 180 (1969); M. Bini, P. G. Bizzeti, A. M. Bizzeti-Sona, and R. A. Ricci, in *Proceedings of the Topical Conference on the Structure of* $1f_{7/2}$ *Nuclei* (see Ref. 67), p. 417.
[k] The 2^+ and 4^+ ^{44}Ca levels are assumed to have pure seniorities $\nu=2$ and 4, respectively.
[l] M. Bini, P. G. Bizzeti, A. M. Bizzeti-Sona, P. Blasi, C. Rossi-Alvarez, and G. B. Vingiani, J. Phys. Soc. Jap. Suppl. 34, 253 (1973).
[m] References 14, 15, and 16.
[n] Reference 21.
[o] The wave functions of MBZ were used to calculate the $B(E2)$ values (Ref. 59).
[p] References 23 and 25.
[q] Reference 16.
[r] B. A. Brown, M. Marmor, and D. B. Fossan, in *Proceedings of the Topical Conference on the Structure of* $1f_{7/2}$ *Nuclei* (see Ref. 67), p. 123; M. Bocciolini, P. Sona, and N. Taccetti, private communication quoted by P. G. Bizzeti, *ibid.*, p. 398.
[s] J. J. Simpson, W. R. Dixon, and R. S. Storey, Bull. Am. Phys. Soc. 18, 603 (1973).
[t] W. R. Dixon, R. S. Storey, and J. J. Simpson, Nucl. Phys. A202, 579 (1973).

lines. The isoscalar effective charge δe_0 obtained using $(fp)^n$ wave functions is especially large for the low-spin $2^+ \rightarrow 0^+$ transitions. This isoscalar enhancement can be explained in terms of core-deformed admixtures which are more important for the low-spin states. The isovector effective charge $\delta e_1 \approx 0.33$, however, is about the same for both high-spin and low-spin transitions.

For the high-spin states the effective proton charge of $1+\delta e_p = 0.96 \pm 0.16$ depends significantly on the amount of $f_{7/2}p_{3/2}$ admixtures in the 4^+ and 5^+ wave functions of ^{42}Ca and ^{42}Sc, respectively. When the wave functions of these states are written as

$$|5^+\rangle = (1-\alpha^2)^{1/2}|(f_{7/2})^2\,5^+\rangle + \alpha\,|(f_{7/2}p_{3/2})5^+\rangle\,,$$

$$|4^+\rangle = (1-\beta^2)^{1/2}|(f_{7/2})^2\,4^+\rangle + \beta\,|(f_{7/2}p_{3/2})4^+\rangle\,,$$

then it is found that

$$e_n = \frac{|[B(E2)]^{1/2}\,{}^{6\rightarrow 4}_{\text{exp}}|}{2.93(1-\beta^2)^{1/2} + 4.60\beta}$$

and

$$e_p = \frac{|[B(E2)]^{1/2}\,{}^{5\rightarrow 7}_{\text{exp}}|}{1.07(1-\alpha^2)^{1/2} + 3.46\alpha} - e_n\,.$$

These results are plotted in Fig. 21 as a function of α for $\beta = 0.59$ and as a function of β for $\alpha = 0.19$. The arrows indicate the amplitudes given by several theoretical calculations.[53,61,62] The arrow labeled FS indicates the value of α and β obtained from the renormalized $(fp)^2$ part of the wave functions given by calculation "B" of Flowers and Skouras.[53] The neutron effective charge varies only slightly as a function of the amplitudes, but the proton effective charge changes by a factor of 4 in the range $\alpha = 0$, a pure $(f_{7/2})^2$ wave function for ^{42}Sc, to $\alpha = 0.60$ which is the approximate $f_{7/2}p_{3/2}$ amplitude in ^{42}Sc given by the three theoretical calculations. The values of the effective charges determined from the various theoretical amplitudes, however, are in fair agreement.

The next level of sophistication for the $42 \leq A \leq 44$ region would be to enlarge the model space even further to include the $2s$-$1d$ shell. Since configurations of the type $(fp)^{n+m}(sd)^{-m}$ are responsible for the core-deformed components which enhance low-spin transitions, the effective charges deduced using this model space depend only on the $\Delta N = 2$ core-polarization excitations. Although no complete calculation of this type has been carried out for these nuclei, a simplified version for the $A = 42$ nuclei has been performed by Flowers and Skouras[53] who considered the configurations $(fp)^2$ and $(fp)^4(sd)^{-2}$. The $B(E2)$ values obtained from the FS paper are given in terms of e_p and e_n in Table II. Adjustments for small differences in the radial matrix elements have been made. These results are plotted graphically in Fig. 22 together with the lines representing the best fits to the high-spin and low-spin transitions. The results of these fits in terms of e_p, e_n, δe_0, and δe_1 are given in Table III. Comparing these FS results with those for the $(fp)^2$ configurations, the isoscalar effective charge for the low-spin transitions is reduced from $\delta e_0 \approx 1.45$ to 0.90. This value is still larger, however, than those obtained for the high-spin transitions ($\delta e_0 \approx 0.31$). The isovector effective charge for both high-spin and low-spin transitions is decreased to $\delta e_1 \approx 0.14$ with the FS wave functions.

B. $48 \leqslant A \leqslant 54$

In this section, the extraction of effective charges for nuclei with $48 \leqslant A \leqslant 54$ will be discussed. Using the $(1f_{7/2})^n$ proton wave functions, the isotones with 28 neutrons can be described very simply since the eight neutrons from a closed shell: $n = \pm 2$ for ^{50}Ti and ^{54}Fe, $n = \pm 3$ for ^{51}V and ^{53}Mn and $n = +4$ for ^{52}Cr. With the present lifetime measurements in ^{54}Fe, ^{53}Mn, and ^{52}Cr, essentially all of the $B(E2)$ values for transitions among these $(1f_{7/2})^n$ proton states have been measured; the results are summarized in Table IV. The calculated $B(E2)$ values and the effective proton charges extracted for $(1f_{7/2})^n$ wave functions are also given in Table IV for each transition. These calculations are straightforward except for a few transitions in ^{52}Cr.

The ^{52}Cr nucleus has two 2^+ and two 4^+ states within the $(1f_{7/2})^4$ configuration,[63] namely those with seniorities $\nu = 2$ and 4. Experimentally there is considerable evidence[64] that the two 2^+ levels are very pure with respect to seniority, the lowest having $\nu = 2$. On the other hand, the branching ratios of the 6^+ level to the two 4^+ levels indicates that their seniority is considerably mixed. With the wave function for the lowest-lying 4^+ level written as

$$|4_1^+\rangle = \alpha\,|(f_{7/2})^4 4^+,\ \nu=2\rangle + (1-\alpha^2)^{1/2}|(f_{7/2})^4 4^+,\ \nu=4\rangle$$

the branching ratios of the 6^+ level[65] can be reproduced only if $\alpha^2 = 0.34$. This substantial seniority mixing can come about through small configuration admixtures of the $2p_{3/2}$ and $1f_{5/2}$ orbitals in the $(f_{7/2})^4\ 4^+$ wave functions. Using the seniority mixed 4^+ wave functions, the calculated $B(E2)$ values involving either of the 4^+ states depend on the known quantity α^2, but not on the unknown phase. For example, the $B(E2)\ (6^+ \to 4_1^+) = (1-\alpha^2) \times B(E2)\ (6^+,\ \nu=2 \to 4^+,\ \nu=4)$ since for half-filled shells the $E2$ operator only connects states with $\Delta\nu = 2$ and the 6^+ state is a pure $\nu = 2$ state. Thus the calculated $B(E2)$ values listed in Table IV for these transitions in ^{52}Cr were obtained with the seniority admixed wave functions ($\alpha^2 = 0.34$).

The transitions between the highest-spin states for the five nuclei from ^{50}Ti to ^{54}Fe yield effective proton charges of 1.88 ± 0.03, 1.94 ± 0.07, 1.83 ± 0.06, $1.94^{+0.17}_{-0.11}$, and 1.98 ± 0.01. These effective proton charges demonstrate additivity by

TABLE III. Effective $E2$ charges obtained for the high-spin ^{42}Ca $6^+ \to 4^+$ and ^{42}Sc $5^+ \to 7^+$ transitions and for the low-spin $A = 42$ $2^+ \to 0^+$ transitions with three different model spaces.

Model space		$(f_{7/2})^2$	$(fp)^2$	$(fp)^2 + (fp)^4\,(sd)^{-2}$
High-spin transitions	e_p	3.81 ± 0.46	0.96 ± 0.16	1.16 ± 0.16
	e_n	0.87 ± 0.02	0.67 ± 0.01	0.45 ± 0.03
	δe_0 [a]	1.84 ± 0.23	0.32 ± 0.08	0.31 ± 0.08
	δe_1 [a]	-0.97 ± 0.23	0.36 ± 0.09	0.14 ± 0.09
$2^+ \to 0^+$ transitions	e_p	2.58 ± 0.26	2.14 ± 0.24	1.76 ± 0.43
	e_n	2.07 ± 0.04	1.73 ± 0.03	1.02 ± 0.10
	δe_0	1.83 ± 0.14	1.44 ± 0.13	0.90 ± 0.24
	δe_1	0.25 ± 0.13	0.30 ± 0.12	0.13 ± 0.20

[a] $\delta e_0 = \frac{1}{2}[e_n + (e_p - 1)]$, $\delta e_1 = \frac{1}{2}[e_n - (e_p - 1)]$.

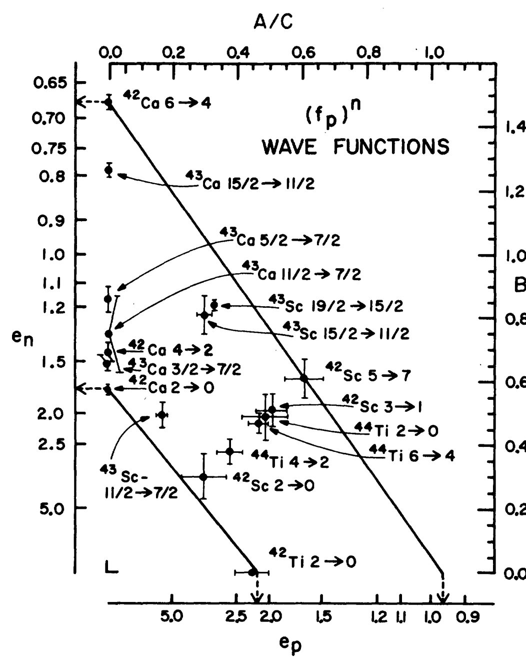

FIG. 20. Plots of the quantities A/C vs B/C with A and B determined from the $(fp)^n$ wave functions of McGrory and Bhatt (Ref. 60). The calculated value $|[B(E2)]^{1/2}|$ is given by $Ae_p + Be_n$, and $C = |[B(E2)]^{1/2}_{\text{expl}}|$. The values of A, B, and C are taken from Table II. The top line is determined by the ^{42}Ca $6^+ \to 4^+$ and ^{42}Sc $5^+ \to 7^+$ transitions and the bottom line represents a fit to the $A = 42$ $2^+ \to 0^+$ transitions. The effective charges given by the axes intercepts are indicated by dashed lines.

being remarkably independent of the number of $1f_{7/2}$ protons. This effect is similar to the fair consistency of the effective neutron charge which was found for the high-spin states in ^{42}Ca and ^{43}Ca using $(1f_{7/2})^n$ neutron wave functions (see Table II). The effective charges for the low-spin states in the isotones with 28 neutrons are not enhanced, which is in contrast to the nuclei near ^{40}Ca where the core-deformed contributions enhance the $B(E2)$ values for the low-spin states. The most serious deviations from constant effective charges for the nuclei with 28 neutrons are for two transitions in ^{53}Mn between low-spin states; however for these, the experimental uncertainties are large and the experimental measurements should be verified. The strongly hindered $\frac{13}{2}^- \rightarrow \frac{11}{2}^-$ $B(E2)$ in ^{53}Mn is not included in the effective charge analysis because, as mentioned in Sec. III, the $\frac{13}{2}^-$ 2563-keV level cannot be a member of the $(1f_{7/2})^{-3}$ configuration and most likely involves a neutron core excitation.

The large number of components in the wave functions for the 28-neutron nuclei using the entire $1f$-$2p$ shell-model space make the calculations prohibitive to carry out. Several simplified calculations have been reported which treat the ^{48}Ca core as closed and which allow only proton excitations.[66] Using these calculated $B(E2)$ values, the effective proton charges are reduced 5–10%; however, the wave functions in these calculations do not have good isospin. The inclusion of excitations from the neutron core to achieve good isospin for the $1f$-$2p$ wave functions improves the consistency between the core-polarization effective charges for the ^{48}Ca region with those for the ^{40}Ca region.[67]

Experimental $B(E2)$ values for transitions in ^{48}Ti, ^{49}V, and ^{50}Cr can also be extracted from the present plunger lifetimes. However, the complexity of these nuclei even in the $(1f_{7/2})^n$ model space makes the results difficult to interpret. Using the MBZ wave functions[59] and $\delta e_p = \delta e_n = 0.6$,

TABLE IV. Comparison of experimental and calculated $B(E2)$ values for transitions in ^{50}Ti, ^{51}V, ^{52}Cr, ^{53}Mn, and ^{54}Fe. The calculated $B(E2)$ values and the resulting effective charges were obtained with $(1f_{7/2})^n$ wave functions. The radial integrals were determined from harmonic oscillator wave functions with $\hbar\omega = 41A^{-1/3}$ MeV.

Nucleus	$J_i \rightarrow J_f$ [a]	$B(E2)_{exp}$ [e^2 fm^4]	Refs.	$B(E2)_{th}$ [e_p^2 fm^4]	e_p [e]
^{50}Ti	$6^+ \rightarrow 4^+$	34.2 ± 1.2	b	9.7	1.88 ± 0.03
	$4^+ \rightarrow 2^+$	60^{+14}_{-10}	c	21.2	$1.69^{+0.19}_{-0.14}$
	$2^+ \rightarrow 0^+$	66 ± 8	d, e	21.3	1.76 ± 0.11
^{51}V	$\frac{15}{2}^- \rightarrow \frac{11}{2}^-$	66 ± 5	c	17.6	1.94 ± 0.07
	$\frac{11}{2}^- \rightarrow \frac{7}{2}^-$	78 ± 14	f, g	23.9	1.80 ± 0.16
	$\frac{9}{2}^- \rightarrow \frac{7}{2}^-$	27.5 ± 6.3	f, g	8.9	1.76 ± 0.21
	$\frac{9}{2}^- \rightarrow \frac{5}{2}^-$	27.5 ± 6.6	f, g	8.3	1.81 ± 0.22
	$\frac{5}{2}^- \rightarrow \frac{7}{2}^-$	154.0 ± 7.6	g, h	52.6	1.72 ± 0.04
	$\frac{3}{2}^- \rightarrow \frac{7}{2}^-$	72 ± 13	g	18.5	1.97 ± 0.18
^{52}Cr	$6^+ \rightarrow 4_1^+$	59.5 ± 3.4	This exp., i	17.7[j]	1.83 ± 0.06
	$6^+ \rightarrow 4_2^+$	30.4 ± 4.5	This exp., i	9.0[j]	1.83 ± 0.06
	$4_2^+ \rightarrow 4_1^+$	92^{+37}_{-24}	k	14.0[j]	$2.56^{+0.48}_{-0.36}$
	$4_1^+ \rightarrow 2_1^+$	83 ± 17	This exp.	18.2[j]	2.14 ± 0.23
	$2_2^+ \rightarrow 2_1^+$	155^{+31}_{-22}	k, l	29.4[j]	2.30 ± 0.19
	$2_2^+ \rightarrow 0_1^+$	≤ 0.2	k, l	0[j]	
	$2_1^+ \rightarrow 0_1^+$	119 ± 7	m	29.1[j]	2.02 ± 0.06
^{53}Mn	$\frac{15}{2}^- \rightarrow \frac{11}{2}^-$	68^{+12}_{-8}	This exp.	18.0	$1.94^{+0.17}_{-0.11}$
	$\frac{11}{2}^- \rightarrow \frac{7}{2}^-$	145 ± 33	f, n	24.6	2.43 ± 0.28
	$\frac{9}{2}^- \rightarrow \frac{7}{2}^-$	96 ± 21	f, n, o, p	9.1	$3.38^{+0.44}_{-0.31}$
	$\frac{9}{2}^- \rightarrow \frac{5}{2}^-$	51^{+15}_{-10}	f, n, p	8.6	$2.45^{+0.34}_{-0.25}$
	$\frac{5}{2}^- \rightarrow \frac{7}{2}^-$	139 ± 26	f, p, q	54.0	1.61 ± 0.15
	$\frac{3}{2}^- \rightarrow \frac{7}{2}^-$	149^{+49}_{-30}	f, n, p	18.9	$2.81^{+0.43}_{-0.30}$

TABLE IV *(Continued)*

Nucleus	$J_i \to J_f$ [a]	$B(E2)_{exp}$ [e^2 fm^4]	Refs.	$B(E2)_{th}$ [$e_p{}^2$ fm^4]	e_p [e]
^{54}Fe	$6^+ \to 4^+$	39.8 ± 0.5	b, r	10.2	1.98 ± 0.01
	$4^+ \to 2^+$	78 ± 16	This exp.	22.3	1.87 ± 0.19
	$2^+ \to 0^+$	102 ± 4	e	22.4	2.13 ± 0.04

[a] Except where noted J_i and J_f refer to states of lowest energy with the respective spins.
[b] Reference 50.
[c] B. A. Brown, D. B. Fossan, A. R. Poletti, and E. K. Warburton, in *Proceedings of the International Conference on Nuclear Physics, Munich,* edited by J. deBoer and P. J. Mang (North-Holland, Amsterdam, 1973), Vol. I, p. 286.
[d] Reference 9.
[e] V. D. Vasil'ev, K. I. Erokhina, and I. Kh. Lemberg, Izv. Akad. Nauk SSSR Ser. Fiz. 26, 1000(1962); [transl.: Bull. Acad. Sci. USSR Phys.Ser. 26, 1000 (1962)] ; J. J. Simpson, J. A. Cookson, D. Eccleshall, and M. J. L. Yates, Nucl. Phys. 62, 385 (1965).
[f] Reference 47.
[g] R. N. Horoshko, D. Cline, and P. M. S. Lesser, Nucl. Phys. A149, 562 (1970); O. F. Afonin, A. P. Grinberg, I. Kh. Lemberg, and I. N. Chugunov, Yad. Fiz. 6, 219 (1967) [transl.: Sov. J. Nucl. Phys. 6, 160 (1968)]; A. W. Barrows, R. C. Lamb, D. Velkley, and M. T. McEllistrem, Nucl. Phys. 47, 506 (1963); H. W. Kendall and I. Talmi, Phys. Rev. 128, 792 (1962); R. N. Horoshko, C. Towsley, and D. Cline, in *Proceedings of the Topical Conference on the Structure of* $1f_{7/2}$ *Nuclei* (See Ref. 67), p. 419.
[h] R. C. Ritter, Phys. Rev. 128, 2320 (1962); I. V. Krause, *ibid.*, 129, 1330 (1963); B. M. Adams, D. Eccleshall, and M. J. L. Yates; I. K. Lemberg; H. E. Gove, and C. Broude, in *Proceedings of the Second Conference on Reactions between Complex Nuclei, Gatlinberg, Tennessee* (Wiley, New York, 1960).
[i] Reference 65.
[j] See Sec. IV B regarding seniority admixtures in the ^{52}Cr states.
[k] Reference 45.
[l] References 42 and 64.
[m] C. W. Towsley, D. Cline, and R. N. Horoshko, J. Phys. Soc. Jap. Suppl., 34, 439 (1973).
[n] Reference 48.
[o] Reference 46.
[p] M. T. McEllistrem, K. W. Jones, and D. M. Sheppard, Phys. Rev. C 1, 1409 (1970); P. H. Vuister, Nucl. Phys. A91, 521 (1967); S. Gorodetsky, F. A. Beck, R. Bertini, E. Bozek, and A. Knipper, Nucl. Phys. 85, 576 (1966); I. M. Szöghy, B. Čujec, and R. Dayrus, Nucl. Phys. A153, 529 (1970).
[q] Reference 49.
[r] Reference 51.

the calculated $B(E2)$ for the ^{48}Ti $6^+ \to 4^+$ transition of 53 e^2 fm^4 agrees with the experimental value of 53 ± 5 e^2 fm^4. The experimental $B(E2)$ values of 144^{+40}_{-25} e^2 fm^4 for the ^{49}V $\frac{11}{2}^- \to \frac{7}{2}^-$ transition and 227 ± 20 e^2 fm^4 for the ^{50}Cr $2^+ \to 0^+$ transition are enhanced by factors of 2.2 and 2.7, respectively, from the calculated values. The $6^+ \to 4^+$ transition in ^{48}Ti seems to be described well by the $(\nu f_{7/2})^{-2}$ $(\pi f_{7/2})^2$ configuration. In ^{49}V and ^{50}Cr the enhanced $B(E2)$ values indicate that effects, such as seniority mixing and excitations to the other $1f$-$2p$ orbitals, are important.

V. CONCLUSIONS

For nuclei near ^{40}Ca, the extracted effective charges exhibit a dependence on the size of the truncated shell-model space from which the wave functions are constructed. Using $(1f_{7/2})^n$ wave functions, the transitions between high-spin levels in ^{42}Ca and ^{43}Ca yield a consistent $E2$ effective charge of $\delta e_n \approx 0.9$; however, similar high-spin transitions in ^{42}Sc and ^{43}Sc yield considerably larger effective charges. An improvement is achieved for the same high-spin transitions by using $(fp)^n$ wave functions; the resulting effective charges then show a consistency for all of the above mentioned nuclei with $\delta e \approx 0.6$ assuming δe for the neutron and proton to be equal. However, the transitions between low-spin states in all of these nuclei show enhanced effective charges using either the $(1f_{7/2})^n$ or $(fp)^n$ wave functions, which reflects admixtures of $2s$-$1d$ core-deformed components.

Neglecting the small orbital dependence of the effective charges, the isoscalar and isovector effective charges in these nuclei near ^{40}Ca can be deduced for the $(fp)^n$ wave functions. For the high-spin transitions, as exemplified by the ^{42}Ca $6^+\to4^+$ and ^{42}Sc $5^+\to7^+$ transitions, an isoscalar effective charge of $\delta e_0=0.32\pm0.08$ is obtained while a $\delta e_0=1.44\pm0.13$ is extracted for the $2^+\to0^+$ transitions in the $A=42$ nuclei. The extracted isovector effective charge $\delta e_1\approx0.33$ is similar for all of these transitions.

In order to obtain the best values for the core-polarization effective charges resulting only from the $\Delta N=2$ particle excitations, the shell-model space has been further enlarged to include the core-deformed components explicitly. Using the wave functions of Flowers and Skouras[53] for the $A=42$ nuclei which include $(fp)^4\,(sd)^{-2}$ components, the isoscalar effective charge for the high-spin transitions remains the same at $\delta e_0=0.31\pm0.08$ while for the low-spin transitions it is reduced to $\delta e_0=0.90\pm0.24$ in comparison to the $(fp)^n$ values. This remaining low-spin enhancement represents an interesting theoretical challenge. The isovector effective charge is reduced to $\delta e_1\approx0.14$ for all transitions in these nuclei near ^{40}Ca.

For the nuclei with 28 neutrons, a consistent effective charge of $\delta e_p\approx0.9$ was obtained for all transitions using $(1f_{7/2})^n$ proton wave functions. This set of results for the five nuclei with $n=2-6$ gives a substantial verification of additivity. It has recently been shown for these nuclei that calculations using good isospin with the $1f$-$2p$ wave functions yield an isoscalar effective charge which is consistent with the best core-polarization value ($\delta e_0\approx0.32$) discussed above for the ^{40}Ca region.[67] The most important correction resulting from the use of wave functions with good isospin comes from the excitation of $1f_{7/2}$ neutrons out of the closed core into the $2p_{3/2}$ orbital. These $\Delta N=0$ corrections are expected to be nearly additive like the $\Delta N=2$ core-polarization contributions.

There has been considerable interest in the core-polarization charges for the ^{40}Ca core and the related giant quadrupole states. The best experimental values are obtained from the high-spin states in ^{42}Ca and ^{42}Sc which are analyzed in terms of the $(fp)^{m+n}(sd)^{-m}$ model space. The results (from Table III) are $\delta e_p^{\rm pol}=e_p-1=0.16\pm0.16$ and $\delta e_n^{\rm pol}=e_n=0.45\pm0.03$ ($\delta e_0=0.31\pm0.08$ and $\delta e_1=0.14\pm0.09$). These were obtained assuming that

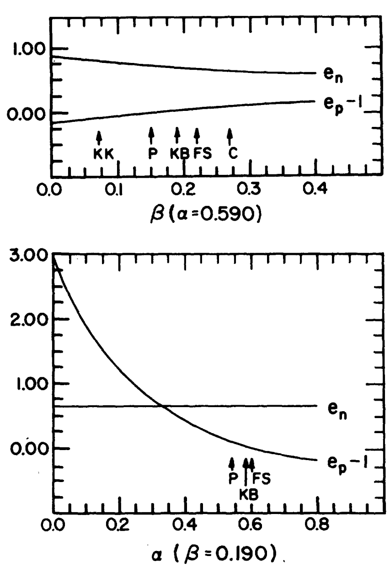

FIG. 21. The quantities e_n and e_p-1 determined from the ^{42}Ca $6^+\to4^+$ and ^{42}Sc $5^+\to7^+$ transitions plotted as a function of α, the amplitude of the $f_{7/2}p_{3/2}$ component of the 5^+ wave function, for $\beta=0.59$ and as a function of β, the $f_{7/2}p_{3/2}$ component of the 4^+ wave function, for $\alpha=0.19$. The arrows indicate the amplitudes given by several theoretical calculations: Flowers and Skouras (FS), Ref. 53; Kuo and Brown (KB), Ref. 61; and Kanestrøm and Koren (KK), Clement (C), and Pühlhofer (P), Ref. 62.

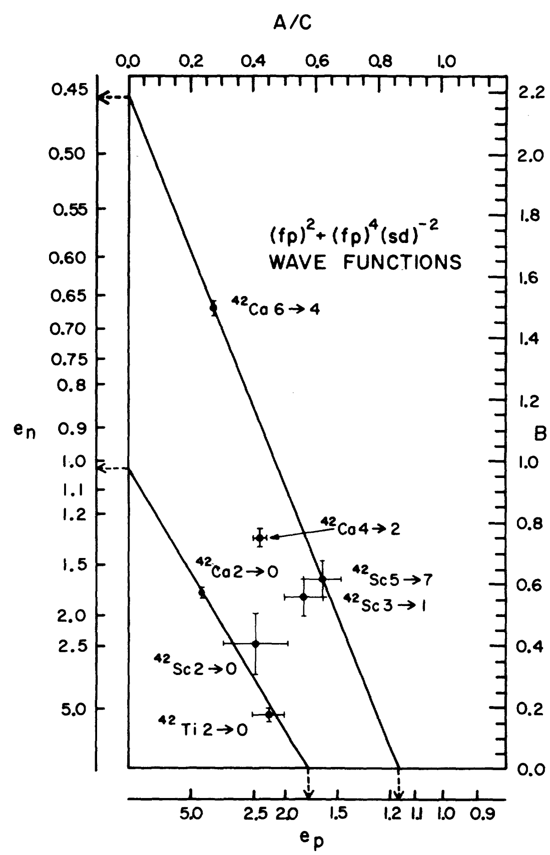

FIG. 22. Plot of the quantities A/C vs B/C with A and B determined from the $(fp)^2+(fp)^4(sd)^{-2}$ wave functions of Flowers and Skouras (Ref. 53). The presentation is similar to that in Fig. 20.

the effective charges are additive as observed experimentally and independent of the orbitals involved. Theoretical calculations indicate that the orbital dependence of δe^{pol} is small in this region.[3] This dependence would not greatly effect these results if it could be explicitly taken into account. These core-polarization effective charges will thus be compared only with theoretical calculations for the $\langle f_{7/2}\|O(E2)\|f_{7/2}\rangle$ matrix element assuming a single particle outside the ^{40}Ca core.

Macroscopic[56,57] as well as microscopic[55] calculations of the core-polarization charges for ^{40}Ca have been made. The macroscopic estimate of Bohr and Mottelson[56] is $\delta e_0 + \delta e_1 \tau_z \approx Z/A + 0.29\tau_z$ ($\tau_z = -1$ for a proton and +1 for a neutron); this expression yields $\delta e_n \approx 0.79$ and $\delta e_p \approx 0.21$. Both the isoscalar and isovector effective charges in this estimate are larger than the experimental values. The macroscopic estimate of Hamamoto[57] is similar to that of Bohr and Mottelson.

Recently, Kuo and Osnes have used several methods to carry out microscopic calculations of the core-polarization charges.[3] A first-order calculation gives $\delta e_0 = 0.28$ and $\delta e_1 = 0.15$ in good agreement with the experimental values. In this order, both the isoscalar and isovector giant quadrupole states in ^{40}Ca lie at ~24 MeV. When these quantities are calculated to second order [random phase approximation (RPA) and Tamm-Dancoff approximation (TDA)], the isoscalar effective charge becomes very large ($\delta e_0 \approx 1.14$ for the RPA); however, the application of self-screening corrections suppresses the collectivity of this isoscalar mode yielding corrected results ($\delta e_0 = 0.40$ and $\delta e_1 = 0.13$ for the RPA) which again are in good agreement with the experimental values. In this second-order calculation, the isoscalar and isovector giant quadrupole states in ^{40}Ca lie at ~19 and ~29 MeV, respectively.

Finally, it is interesting to compare our results with a similar analysis of the $h_{9/2}$ polarization charges in the ^{208}Pb region by Astner *et al.*[2] They obtain $\delta e_0 = 0.63 \pm 0.03$ and $\delta e_1 = 0.10 \pm 0.03$. The isovector polarization charge agrees with our value, while the isoscalar value is larger than our result of $\delta e_0 = 0.31 \pm 0.08$. These values for δe_0 do not follow the Z/A estimate of Bohr and Mottelson.[56]

ACKNOWLEDGMENTS

The authors would like to thank A. Arima for helpful theoretical discussions, J. B. McGrory for sending the $(fp)^n$ matrix elements, I. Plesser for his help on the initial phases of the experiment, and R. McKeown for his help with the data analysis and figure preparation.

---

*Work supported in part by the National Science Foundation.

†Present address: at the Sloan-Kettering Laboratories, New York, New York.

‡Present address: at the Physics Department, University of Washington, Seattle, Washington.

[1]A. Bohr and B. Mottelson, *Nuclear Structure* (Benjamin, New York, 1969), Vol. 1, Chap. 3.

[2]G. Astner, I. Bergström, J. Blomqvist, B. Fant, and K. Wikström, Nucl. Phys. A182, 219 (1972).

[3]T. T. S. Kuo and E. Osnes, Nucl. Phys. A205, 1 (1973).

[4]T. K. Alexander, K. W. Allen, and D. C. Healey, Phys. Lett. 20, 402 (1965).

[5]K. W. Jones, A. Z. Schwarzschild, E. K. Warburton, and D. B. Fossan, Phys. Rev. 178, 1773 (1969).

[6]D. B. Fossan and E. K. Warburton, in *Nuclear Spectroscopy II*, edited by J. Cerny (Academic, New York, 1974), Chap. VII. H., p. 307.

[7]D. Ashery, N. Bahcall, G. Goldring, A. Sprinzak, and Y. Wolfson, Nucl. Phys. A101, 51 (1967).

[8]A. Abragam and R. V. Pound, Phys. Rev. 92, 943 (1953).

[9]O. Häusser, D. Pelte, T. K. Alexander, and H. C. Evans, Nucl. Phys. A150, 417 (1970).

[10]B. A. Brown, J. M. McDonald, D. B. Fossan, K. A. Snover, and I. Plesser, Bull. Am. Phys. Soc. 16, 1178 (1971).

[11]J. M. McDonald, B. A. Brown, K. A. Snover, D. B. Fossan, and I. Plesser, Bull. Am. Phys. Soc. 16, 1183 (1971).

[12]B. A. Brown, J. M. McDonald, and K. A. Snover, Bull. Am. Phys. Soc. 17, 583 (1972).

[13]B. A. Brown, J. M. McDonald, K. A. Snover, and D. B. Fossan, Bull. Am. Phys. Soc. 17, 933 (1972).

[14]N. R. Roberson and G. Van Middelkoop, Nucl. Phys. A174, 577 (1971).

[15]D. P. Balamuth, G. P. Anastassiou, and R. W. Zurmühle, Phys. Rev. C 2, 215 (1970).

[16]R. Hartman, H. Grawe, and K. Kändler, Nucl. Phys. A203, 401 (1973).

[17]R. Sherr, T. D. Bhatia, D. Cline, and J. J. Schwartz, Ann. Phys. (N. Y.) 66, 548 (1971); F. M. Nicholas, N. Lawley, I. G. Main, M. F. Thomas, and P. J. Twin, Nucl. Phys. A124, 97 (1969).

[18]M. C. Bertin, G. J. Kumbartzki, and R. G. Hirko, Nucl. Phys. A192, 524 (1972).

[19]W. J. Kossler, J. Winkler, and C. D. Kavaloski, Phys. Rev. 177, 1725 (1969).

[20]T. K. Alexander, Phys. Lett. 20, 402 (1966).

[21]K. Nakai, B. Skaali, N. J. S. Hansen, B. Herskind, and Z. Sawa, Phys. Rev. Lett. 27, 155 (1971).

[22]W. P. Alford, N. Schulz, and A. Jamshidi, Nucl. Phys. A174, 148 (1971).

[23]C. P. Poirier, A. Tveter, J. C. Manthuruthil, J. Walinga, V. E. Storizhko, and B. D. Kern, Phys. Rev. C 3, 1939 (1971).

[24]J. S. Forster, G. C. Ball, F. Ingebretsen, and C. F. Monahan, Phys. Lett. 32B, 451 (1970).

[25]G. C. Ball, J. S. Forster, F. Ingebretsen, and C. F.

Monahan, Nucl. Phys. A180, 517 (1972).
[26]T. A. Critchley and W. R. Phillips, Phys. Lett. 25B, 328 (1967).
[27]G. C. Ball, J. S. Forster, D. Ward, and C. F. Monahan, Phys. Lett. 37B, 366 (1971).
[28]N. Lawley, N. Dawson, G. D. Jones, I. G. Main, P. J. Mulhern, R. D. Symes, and M. F. Thomas, Nucl. Phys. A149, 95 (1970).
[29]D. H. White and R. E. Birkett, Phys. Rev. C 5, 513 (1972).
[30]H. Gruppelaar and P. J. M. Smudlers, Nucl. Phys. A179, 737 (1972); J. D. McCullen and D. J. Donahue, Phys. Rev. C 8, 1406 (1973).
[31]P. Fettweis and M. Saidane, Nucl. Phys. A139, 113 (1969).
[32]J. Konijn, E. W. A. Lingeman, and S. A. DeWit, Nucl. Phys. A90, 558 (1967).
[33]C. D. Kavaloski and W. J. Kossler, Phys. Rev. 180, 971 (1969); T. T. Bardin, J. A. Becker, and T. R. Fisher, Phys. Rev. C 7, 190 (1973).
[34]P. Blasi, M. Mandó, P. R. Maurenzig, and N. Taccetti, Nuovo Cimento 4A, 61 (1971).
[35]Z. P. Sawa, J. Blomqvist, and W. Gullholmer, Nucl. Phys. A205, 257 (1973).
[36]J. N. Mo, B. Čujec, R. Dayras, I. M. Szöghy, and M. Toulemonde, Nucl. Phys. A147, 129 (1970).
[37]H. C. Cheung and S. K. Mark, Nucl. Phys. A176, 219 (1971); G. B. Vingiani, C. Rossi-Alvarez, A. Buscemi, F. Brandolini, and F. Cervellera, Phys. Lett. 40B, 638 (1972).
[38]C. M. Rozsa, R. G. Arns, B. J. Brunner, S. E. Caldwell, and J. W. Smith, Bull. Am. Phys. Soc. 17, 604 (1972); and private communication.
[39]A. Kiuru, Z. Phys. 251, 93 (1972).
[40]S. Raman, R. L. Auble, W. T. Milner, J. B. Ball, F. K. McGowan, P. H. Stelson, and R. L. Robinson, Nucl. Phys. A184, 138 (1972).
[41]W. Dehnhardt, O. C. Kistner, W. Kutschera, and H. J. Sann, Phys. Rev. C 7, 1471 (1973).
[42]P. A. Assimakopoulas, T. Becker, Cyrus Moazed, and D. M. Van Patter, Nucl. Phys. A180, 131 (1972).
[43]I. Forsblom, T. Weckström, T. Sundius, G. Bergström, S. Forss, and G. Wansén, Phys. Scr. 6, 309 (1972).
[44]J. W. Noé, R. W. Zurmühle, and D. P. Balamuth, Bull. Am. Phys. Soc. 18, 653 (1973); and private communication.
[45]S. W. Sprague, R. G. Arns, B. J. Bunner, S. E. Caldwell, and C. M. Rozsa, Phys. Rev. C 4, 2074 (1971).
[46]Z. P. Sawa, Phys. Scr. 7, 5 (1973).
[47]A. S. Goodman and D. J. Donahue, Phys. Rev. C 5, 875 (1972).
[48]F. Brandolini, A. Brusegan, C. Signorini, and R. A. Ricci, Nuovo Cimento 7A, 144 (1972).
[49]S. Gorodetzky, N. Schulz, E. Bozek, and A. Knipper, Nucl. Phys. 85, 519 (1966).
[50]T. Nomura, C. Gil, H. Saito, T. Yamazaki, and M. Ishihara, Phys. Rev. Lett. 25, 1342 (1970); S. Cochavi, D. B. Fossan, S. H. Henson, D. E. Alburger, and E. K. Warburton, Phys. Rev. C 2, 2241 (1970).
[51]R. Hensler, J. W. Tape, N. Benczer-Koller, and J. R. MacDonald, Phys. Rev. Lett. 27, 1587 (1971).
[52]W. J. Gerace and A. M. Green, Nucl. Phys. A93, 110 (1967).
[53]B. H. Flowers and L. D. Skouras, Nucl. Phys. A136, 353 (1969).
[54]C. W. Towsley, D. Cline, and R. N. Horoshko, Phys. Rev. Lett. 28, 368 (1972); Nucl. Phys. A204, 574 (1973).
[55]H. Noya, A. Arima, and H. Horie, Prog. Theor. Phys. Suppl. 8, 33 (1958); P. Federman and L. Zamick, Phys. Rev. 177, 1534 (1969); S. Siegel and L. Zamick, Phys. Lett. 28B, 450, 453 (1969); Nucl. Phys. A145, 89 (1970); A. E. L. Dieperink and P. J. Brussaard, *ibid.* A129, 33 (1969); M. Harvey and F. C. Khanna, *ibid.* A164, 612 (1971); P. Goode, B. J. West, and S. Siegel, *ibid.* A187, 249 (1972); R. W. Sharp and L. Zamick, *ibid.* A208, 130 (1973).
[56]A. Bohr and B. Mottelson, *Nuclear Structure* (Benjamin, New York, to be published), Vol. II, Chap. 6.
[57]I. Hamamoto, in Supplementary Research Report of Laboratory of Nuclear Science, Tohoko Univ. 5, 205 (1972).
[58]H. R. Collard, L. R. B. Elton, and R. Hofstadter, in *Landolt-Bornstein Numerical Data and Functional Relationships in Science and Technology,* edited by K.-H. Hellwege and H. Schopper (Springer-Verlag, Berlin, Germany, 1967), New Series, Group I, Vol. 2.
[59]J. D. McCullen, B. F. Bayman, and L. Zamick, Phys. Rev. 134, B515 (1964).
[60]K. H. Bhatt and J. B. McGrory, Phys. Rev. C 3, 2293 (1971); J. B. McGrory, *ibid.* 8, 693 (1973); and private communication.
[61]T. T. S. Kuo and G. E. Brown, Nucl. Phys. A114, 241 (1968).
[62]I. Kanestrøm and H. Koren, Nucl. Phys. A130, 527 (1969); D. M. Clement, *ibid.* A132, 49 (1969); F. Pühlhofer, *ibid.* A116, 516 (1968).
[63]C. Schwartz and A. de-Shalit, Phys. Rev. 94, 1257 (1954).
[64]G. Kaye and J. C. Wilmott, Nucl. Phys. 71, 561 (1965); P. M. Van Patter, N. Nath, S. M. Shafroth, S. S. Malik, and M. A. Rothman, Phys. Rev. 128, 1246 (1962).
[65]A. Pakkanen, Ann. Acad. Sci. Fenn. A253, 1 (1967); M. S. Freedman, F. Wagner, F. T. Porter, and H. H. Bolotin, Phys. Rev. 146, 791 (1966).
[66]B. Barman Roy, R. Raj, and M. L. Rustgi, Phys. Rev. C 1, 207 (1970); M. L. Rustgi, R. P. Singh, B. Barman Roy, R. Raj, and C. C. Fu, *ibid.* 3, 2238 (1971); K. Lips and M. T. McEllistrem, *ibid.* 1, 1009 (1970); K. Lips, *ibid.* 4, 1482 (1971); T. Komoda, Nucl. Phys. 51, 234 (1964).
[67]A. Arima, B. A. Brown, and J. B. McGrory, to be published; other aspects of good-isospin wave functions are discussed by E. Osnes and C. S. Warke, Nucl. Phys. A154, 331 (1970) and E. Osnes, in *Proceedings of the Topical Conference on the Structure of* $1f_{7/2}$ *Nuclei,* edited by R. A. Ricci (Editrice, Bologna, 1971), p. 79.